Modeling the *cutter head-rock* interaction to simulate the dynamic cutting process

Lode Vancauwenbergh

CONFIDENTIAL

Delft University of Technology
Section of Dredging Engineering

version 4.1 December 7, 2016

Modeling the *cutter head-rock* interaction to simulate the dynamic cutting process

Author:

Lode Vancauwenbergh 4315995

Thesis Committee:

Prof. Dr. Ir. C. van Rhee	Delft University of Technology
Dr. Ir. S.A. Miedema	Delft University of Technology
Dr. Ir. M. Janssen	Delft University of Technology
Dr. Ir. D.J.M. Ngan-Tillard	Delft University of Technology
Ir. F. De Corte	DEME - Dredging International NV
Ir. S. Claessens	DEME - Dredging International NV

TU Delft
Delft University of Technology

DEME
Dredging, Environmental & Marine Engineering

In collaboration with DEME - Dredging International NV and Delft University of Technology

This page is intentionally left blank.

Abstract

Context The construction of growing maritime infrastructure often requires the deepening of approach channels or berths to create the access for large ships. The seabed can consists of different types of materials. For each type of material (sand, clay and rock), a different excavation technique is required. During the excavation of hard rock (up to 60 MPa), existing cutter suction dredgers reached there working limits. When a cutter suction dredger was no longer capable of excavating the rock, explosives were used in the past to demolish the hardest rock parts. Environmental issues in the last decades have led to a very strict legislation concerning the marine habitat and a ban on the use of explosives in certain areas. This forced dredging contractors to explore alternative approaches to excavate the hardest rock types.

Problem definition High amplitude vibrations occurred during the excavation of hard rock types in the past. These vibrations have resulted among other to the failure of gearboxes and the pontoon's structure. High repair costs made these projects no longer profitable. Many dredging contractors approached this problem by building stronger cutter suction dredgers and cutter heads, but the question remains whether this is the solution. A better understanding of the rock cutting process could lead to a more efficient way of excavating rock.

Until now, the excavation of hard rock types using a cutter suction dredger was an unpredictable process. The character of the irregular cutting process is unknown and no direct relation is found between feasibility, production rates and rock strength characteristics. During the execution of hard rock type projects, high wear rates were encountered. No valuable explanation was found for these high values, leading to an unpredictable consumption of cutting teeth. This has led to inaccurate production calculations and wrong estimations of the costs involved during a project.

The unpredictable character of rock excavation forced dredging contractors to analyze the process in more detail. The first step in the further analysis of the excavation of hard rock with a cutter suction dredger is the modeling of the interaction of the cutter head and rock. The great need for this modeling led to the conduct of this research.

Approach This report includes an investigation into the interaction between a cutter head of a cutter suction dredger and rock. A discrete model is built to simulate the interaction phenomena including the formation of rock chips and the forces generated. The goal of the research is to approximate the irregular cutting process of rock as accurate as possible. The theoretical approach of rock cutting is applied within the discrete model. The physical background of rock cutting as well as the discrete model is discussed in this research. A discrete model is used to limit the computation time of a run. A disadvantage of the discrete model is the limited accuracy.

The model is calibrated and validated by field tests. Real-time torque measurements are used to investigate the reliability of the model. Field tests consist of torque measurements performed on the cutter shaft of a cutter suction dredger. To generate a representative output signal from the model, a simplified dynamic model of the cutter drive train was implemented. Several cases are run afterwards to investigate the effect of dredge, cutter head and cutting tooth parameters. These cases are based on issues encountered during the dredging of rock and try to interpret the cause of a specific phenomenon.

Results and conclusions The model shows great similarities with the reality. The torque measurements on board different types of cutter suction dredgers and for different rock types were validated and the emergent phenomena were recognized in the simulated torque output signal of the model. It can therefore be concluded that the model consists of a stable rock interaction module and a reliable dynamic model.

The model can be used to predict the forces encountered and wear of cutting teeth. This allows a dredging contractor to estimate the consumption of cutting teeth during a project. Another implementation of the model is the prediction of feasible production rates. The limitations of a cutter suction dredger can be tested beforehand the execution of a project based on torque and forces present during the excavation of a specific rock type. The different behavior of several types of cutter heads can be modeled, as well as their ideal working point can be investigated. The dynamic model allows the user to investigate the effect of torsional vibrations induced on the cutter shaft.

The model enables a dredging contractor to investigate the rock-cutter head interaction and optimize the rock excavation process. Influencing parameters can be examined during the execution of a project. The insight gained in the cutter head-rock interaction finally leads to a better estimation of a dredging project, saving excess charges before, during and after the execution of a project.

Preface

This research report is written to obtain the degree of Master of Science at the faculty of Dredging Engineering of the Delft University of Technology. During my study, I noticed that modeling and programming dredging processes nowadays can lead to highly accurate approximations of the reality. This seemed like a great challenge to me and I decided to further specialize myself within the field of programming numerical models.

My background as a nautical officer on board delivers me practical insight in the maritime industry. This practical knowledge combined with the theoretical background that I achieved at the Delft University of Technology, formed a good base to assess maritime/mechanical processes. DEME offered me an extensive research project concerning a model to simulate the excavation of rock with a heavy duty rock cutter. This research project drew my attention due to the combination of the civil and mechanical engineering fields. I like the idea of solving tangible problems with well-tailored software to advance the field of dredging engineering. Therefore the research project aroused my enthusiasm to develop new ideas and push boundaries.

After performing a literature study on the excavation of hard rock types with cutter suction dredgers, I noticed the inability of many software packages to efficiently model the excavation process. The use of DEM (Discrete Element Modeling) requires too high computation times to make a simulation achievable. For this reason, I decided to create a simplified version of the DEM-method and which was able to simulate the cutter head-rock interaction as accurate as possible within a time period of hours. One of the most important aims of the project was to model the dynamic behavior of the cutter drive train and couple the effects with the excavation process. This dynamic interaction is a crucial issue in current cutter suction dredger design.

I hope that this research contributes to the dredging science and helps researchers and dredging contractors to gain more insight in the excavation process of hard rock types with a cutter suction dredger. By use of the software, engineers should be able to test many more research cases than already discussed in this report. The cases can be related to achievable production rates and design criteria of a cutter suction dredger.

Lode Vancauwenbergh
Antwerpen,
December 1, 2016

Aknowledgements

This research would not have led to the same results without the help and commitment of many persons. In this short note in front of the report, I want to thank all of them who contributed to the results of this research project.

Special thanks goes out to the dredging contractor DEME and sub contractor Dredging International who provided me during a year with an office and a nice surrounding atmosphere and colleagues. Within this company, I want to thank Ir. Stijn Claessens for his weekly professional advice during our 'progress problems plans'-meeting. Furthermore, I want to thank Ir. Marc van den Broeck, Ir. Kobe Paridaens, Ir. Arnaud Verschelde and Ir. Wannes van Beneden for their help and support during the research project.

I am very grateful to the Delft University of Technology for providing me with all the knowledge I have obtained during my study. Special thanks goes out to Prof. Dr. Ir. C. van Rhee and Dr. Ir. S.A. Miedema. The monthly and three-monthly meetings were an indispensable feedback moment. Their professional advice contributed to a large extent to the results obtained in this research.

Last but not least, I want to thank my family and girlfriend. First of all, my greatest admiration goes out to my girlfriend Elke Geens who survived my obsession with my computer and was there for me every evening and during all difficult times I encountered. I am grateful to my parents, sister and brother in law who gave me great encouragement. Thank you Stefan Dirven, for the good times we had at the Delft University of Technology and the support during this research project. Last but not least, special thanks goes out to all my friends for their support and useful information and feedback I received from them (especially Annelies and Joris on their world tour, see picture below).

Lode Vancauwenbergh
Antwerpen,
December 1, 2016

Contents

Chapter 1

Introduction

Due to the increasing demand for port construction, expansion, the installation of infrastructure at sea and the construction of inland waterways, the excavation of rock became an inevitable part of the dredging industry in the last decades. Some areas in the world possess rocky coasts (f.e. Panama, see figure 1.1). Nevertheless, these regions are forced to create harbors, sea lanes or canals to create access for ships and compete in the international economy. The increasing amount and size of ships did rise the demand to excavate more and harder types of rock at the seabed.

Figure 1.1: Rock excavation project in Panama.

The excavation of rock on the seabed is a technique of dredging developed from the sixties on. The dredging of rock is a craft largely based on experience. Rock is a challenging material to dredge as it has a completely different failure behavior than the typical materials dredging companies are used to work with (sand and clay). The physical behavior is unpredictable and irregular, which tends dredging contractors to approach rock dredging by a simple rule of thumb: stronger rock is to be dredged by a stronger machine. Nevertheless, the question remains whether this is true or not.

The excavation of rock can be done using several types of dredgers, which are classified as hydraulic or mechanic dredgers. The mechanic dredgers use different types of grabs and can only excavate the softer rock types or rock which is already fragmented. Rock fragmentation is sometimes executed prior to the excavation by drilling and blasting methods[1]. Drilling and blasting is often environmentally not allowed and is cost-effective not an optimal solution due to the twofold execution stage. Hydraulic dredgers use a suction pipeline to displace the rock. This research only considers cutter suction dredgers, which is a combination of a mechanic and hydraulic dredger (see figure 1.3) whereby the cutting is executed mechanically and the displacement is performed by a suction pipeline. Only the excavation process is further investigated.

[1]Drilling and blasting is the breakage of rock by the controlled use of explosives and other methods such as gas pressure blasting pyrotechnics

During the tendering phase of a project, dredging companies estimate the costs involved to execute a project and set up a bidding. The decision whether a project is executable with a certain cutter suction dredger or not is now based on similar projects executed in the past. In a short period prior to the project, an estimation must be made about the dredging equipment to be used, the expected production rate and the cost of wear parts. It is clear that the type of rock encountered is one of the most important parameters in assessing a project. Often, not many rock properties are given by the client and dredging companies face the challenge to estimate the rock type and fracturing as good as possible. Geologists create a soil model which matches the field samples delivered by the client. This soil model is a horizontal and vertical distribution of soil properties over the area to be dredged. Based on the soil model, production estimation engineers decide which type of equipment can execute the project and can deliver the highest production rate. A good knowledge of the behavior of cutter suction dredgers in a specific rock type is therefore required.

Figure 1.2: The strongest cutter dredger ever built: Ambiorix (http://www.deme-group.com (2016))

In the last decade, more dredging projects consist of excavating very hard rock types like basalt[2]. When hard to very hard rock types were encountered in the past, modern cutter suction dredgers have reached their operational limits. More insight in the excavation process is required to shift the boundaries of current cutter suction dredgers. A rock excavation prediction tool is needful to estimate an excavation work beforehand when limited feed back data is available from comparable projects in the past. This knowledge is required to keep competing with other dredging companies and being capable of excavating rock types never dredged by a cutter suction dredger.

1.1 The dredging contractor DEME

DEME (Dredging, Environmental and Marine Engineering) was established in 1991, but the roots of the company date back in the 19^{th} century. In the early years, Baggerwerken Decloedt (as DEME's earliest predecessor was called) was a small dredging company along the Belgian coast. In 1974, the well known Dredging International was founded as a merger between dredging contractors Ackermans & van Haaren and Sociéte Générale de Dragage (SGD). DEME is established as a holding company between the two Belgian dredging contractors Dredging International and Baggerwerken Decloedt. In 2016, DEME is a

[2]Basalt is a common extrusive igneous (volcanic) rock formed from the rapid cooling of basaltic lava.

worldwide player on the dredging market and employs over 4 600 people. Although DEME's activities originated with its core dredging business more than 140 years ago, they have broadened their portfolio substantially over the last decades. Today, the activities encompass dredging, land reclamation, hydraulic engineering, services for the offshore oil, gas and renewable energy sectors and environmental works (http://www.deme-group.com (2016)).

DEME owns a fleet of all types of vessels to execute maritime and inland water works. DEME's fleet now includes 90 major ships and some 200 auxiliary vessels. Among these vessels, the cutter fleet consist of 14 major pontoons. Among them are the strongest cutter dredgers ever built, the D'Artagnan and Ambiorix, two self-propelled 28,200 kW seagoing, mega rock cutters (http://www.deme-group.com (2016)).

1.2 Problem statement

This research considers the excavation of hard rock types performed by a heavy duty cutter suction dredger. The working principle of a cutter suction dredger is explained in chapter 2. In the further course of this introduction, some terms may be used which are further discussed in chapter 2.

The rising demand to dredge increasingly stronger rock has uncovered the details of the excavation process. Intact rock material is only economically feasible to be dredged with a heavy duty cutter suction dredger when the Unconfined Compressive Strength (UCS) is not exceeding 60 MPa, although rock types with an UCS of up to 150 MPa are currently dredged when they are in fragmented condition. All depends on the state of the rock mass. When the UCS value of rock types exceeds the upper boundary of 60 MPa

Figure 1.3: Sketch of a cutter suction dredger excavating rock (http://www.deme-group.com (2016))

compressive strength, many unwanted issues occur during the excavation. The irregular cutting process creates an unevenly loaded cutter shaft which is continuously decelerating and accelerating. A consequence of the irregular character of the process is the introduction of vibrations, causing damage to the gearbox of the cutter drive and pontoon's structure. In rare cases where very hard rock types are encountered exceeding the limitations, the cutter head can stall or even run over the bank[3] in stead of digging in.

DEME analyzed these problems and stated that a great improvement could already be obtained by redesigning the cutter head. Several new types of cutter heads were built and tested by DEME to reduce

[3]A bank is the volume of uncut rock mass being excavated

excessive vibrations on board. Torque measurements on the cutter shaft and vibration analyzes where performed to measure the influence of the cutter head type on the excavation process. Drawing conclusions was challenging, because in practice it is rarely possible to perform field tests where all influencing parameters are exactly known and kept constant. DEME decided that there was a need to physically model the influence of dredge parameters and cutter head type on the excavation process. This modeling could further optimize the project estimation beforehand and could visualize the effective influence which the new designed cutter heads have.

The vibration problems encountered during the excavation of rock raises many question. These vibrations are harmful for rotary equipment and the pontoon's structural strength. On the other hand, these vibrations may be inevitable for the excavation process to generate the hammering effect and incorporate the inertia[4] effect of the cutter head. It may become clear that the solution is not simply found in reducing the vibrations. A detailed analysis of the process and behavior of the drive train in loaded condition is required. The research question is therefore stated as follows:

How does the cutter head-rock interaction influences the dynamic cutting process?

Starting from this major research question, several spin-off questions are formulated. What influence does the cutter head type has on the cutting process? What impact does the wear of cutting teeth have on the cutting process? What influence do torsional vibrations have on the cutting process? For all these questions, this research is required to give an explanation.

(a) Unused cutter head with sharp teeth (b) Damaged cutter head and damaged/worn teeth

Figure 1.4: A cutter head before and after a hard rock excavation work

1.3 Problem approach

The approach of this research is to model the interaction of a cutter head in contact with rock. The cutter head parameters must be interchangeable as well as the pontoon's characteristics. The wear of cutting teeth is considered. During the modeling of the cutter head-rock interaction, dredge parameters must be varied to investigate which effect they have. A simplified dynamic model of the cutter shaft and drive is built to incorporate the dynamic behavior of the cutter head drive train.

A discrete model is applied because of the irregular breakout pattern of rock shapes. Discrete modeling means that motions are continuous but are a sequence of positions, whereby the position interval is defined as the accuracy of the model. In this model, an accuracy of 1 centimeter is applied.

[4]Inertia is the resistance of any physical object to any change in its state of motion; this includes changes to its speed, direction or state of rest.

To model the cutter head-rock interaction, a geometric model of the cutter head is required. This geometric model incorporates the complete geometry and motions of a cutter suction dredger. The next step is setting up a rock model. This rock model can be shaped as desired relative to the moving cutter head and user-defined rock properties are added. Combining the geometric simulation with a rock model, the interaction can take place. The interaction of cutter head and rock is modeled as accurate as possible. The interaction module consists of several submodules. The forces generated as well as the volumes of rock being excavated are simulated and stored.

The model is built to be modular. This implies that each part of the model can be plugged in or out. The purpose of this modular structure of the model is the further implementation as a part of complete dynamic model of a cutter suction dredger. The model is calibrated and validated using field test data to ensure the reliability. After validation of the model, parameters can be varied to investigate their influence and scope of the simulation model.

The main and general aim of the simulation is to investigate which type of cutter head performs optimal during certain rock conditions. To categorize which cutter head performs best considering rock properties, several parameters must be compared against each other due to the variety of influencing parameters on the excavation process. The intention of this research is not to redesign cutter heads, but to investigate the influencing parameters and create a stable simulation model.

1.4 Outline of the thesis

This report serves as a theoretical manual for the model which was built to simulate the cutter head-rock interaction. The theoretical background of the assumptions made in the model are discussed. To provide the reader of this research with a compact, easy to read and complete document, the report only consists of the most inevitable information to understand the excavation of rock. For more in depth information is referred to the appendices. The body of this thesis consists of four main parts: the geometric model, the rock model, the cutter head-rock interaction and the validation of the results. In advance, the general working method of a cutter suction dredger is explained and last but not least, a final conclusion is stated at the end.

The geometric model covers the discrete modeling of all positions, directions and shapes required to simulate a cutter suction dredger and its cutter head. The goal of this chapter is to give the reader a clear overview of all separated motions which contribute to the total path traveled by the cutting teeth. Different reference frames are required to define all positions and orientations in space and time. A correlation is set up between these reference frames to make transformations possible.

A rock model is discussed in the next chapter. The model must be a good representation of the reality despite the fact that only limited rock parameters are known in advance of a project. The interpretation and simplification of a specific rock type is investigated. The theoretical cutting process of a cutting tooth in rock is examined. The implementation of this theoretical approach in a three-dimensional space and the assumptions which are required to do so are discussed.

Chapter 2

Working method of a cutter suction dredger

A dredger is often required during the construction of ports and waterways when rock is to be moved. The dredger is brought in position and starts excavating rock following a predefined production scheme. Cutter suction dredgers are pontoons equipped with a rotation device to loosen rock. This rotation device, called a cutter head, is mounted in front of a suction mouth, all positioned at the end of a ladder which can be lowered to the seabed. The ladder is attached to the pontoon by a hinge at the top edge. The loosened rock is sucked up as a mixture with water through a suction mouth and transported by a suction pipeline. The suction force is obtained by using (a) powerful suction pump(s) located under water and/or in the pontoon's pump room. The suction and/or booster pumps send the mixture of rock and water through a discharge pipeline to a reclamation area or barge. The cutter suction dredger is stationary and anchored while dredging. During the cutting process, the dredger swings back and forth around a fixed point on the stern, which is called the working spud. The working spud is the aft anchoring point. The swing motion is initiated by anchors and winches. The anchors are positioned in front of the dredger with a certain offset from the center line. Side wires connected to these anchors are hauled or veered by winches on the forward deck, introducing a rotating motion around the working spud.

The excavation process in rock is characterized by a high variation in excavation forces, which requires a rigid anchoring of the pontoon. Excavation forces are transferred towards the seabed by the anchors and working spud. The cutter suction dredger will mostly be used in sheltered areas to reduce the effect of waves and swell. Almost all soil types, including strong rock, can be excavated. Dredging depths from 1 to 35 meters can be reached. The power available at the cutter head goes up to 6000 kW for the strongest cutter suction dredgers.

2.1 The cutter head

Different types of rock require different types of cutter head. Each cutter head is designed to require minimal energy to reach a certain production and being most cost-effective for a specific rock type. The design is based on practical experience and laboratory tests. The cutter head is driven by the cutter head shaft. A cutter head consists of four main parts (see figure 2.1):

- a back ring (gray part)
- a hub (red part)
- a number of blades (orange parts)
- a number of cutting teeth (yellow parts)

The hub is the connection of the cutter head to the cutter head shaft. Blades connect the hub with the back ring. The number of blades depends on the rock type to be excavated. Less blades create big

Figure 2.1: Cutter head drawing

openings between the blades which allows high production rates. On the contrary, bigger rock parts will enter the pipeline which may create blockages in the pump. Plates or bars can be mounted between the cutter head blades to prevent or break excavated parts in smaller pieces. More blades will mean that a smaller slice thickness is encountered and excavation forces per cutting tooth are reduced. Adapters are mounted on the blades and serve as a base for the cutting teeth. Teeth exist in various shapes and sizes, are subject to wear phenomena and are replaceable. A example is shown in figure 2.2.

Figure 2.2: Cutting teeth mounted on a cutter head

Depending on the rock type being dredged, the cutter head must be replaced frequently during cutter head checks. Damage occurs to the cutter head, adapters and teeth when the cutter head is unevenly loaded with high peaks.

2.2 The cutter ladder

The purpose of the cutter ladder is to position the cutter head at the required cutting depth and transfer the forces towards the pontoon. One end of the ladder is attached to the pontoon with a hinge by which it can rotate vertically. The end where the cutter head is mounted is connected to a hoisting cable. Winches located at the pontoon can haul or veer the hoisting cable to rotate the cutter ladder around

Figure 2.3: The cutter head mounted on the cutter ladder

its hinge point. Cutter head ladders considered in this thesis are box-shaped structures. This design can withstand peak loads much easier than an open frame construction. Most of the cutter ladders are tapered towards the cutter head. The cutter head end of the ladder must be as small as the cutter head back ring diameter. This prevents the cutter head ladder to touch uncut rock. Near the hinge point, the box-shaped ladder is much bigger to transfer the forces towards the pontoon. At this end, the cutter head drive and side winches can be positioned.

The cutter ladder is equipped with side wire sheaves. These sheaves guide the side wires and are attached to the ladder near the cutter head. The position of the anchors varies with respect to the cutter head, which requires the side wire sheaves to pivot according to the angle that is formed by the side wire relative to the ladder. The position of the side wire sheaves on the ladder determines the point of application of the hauling force on the ladder. The sheaves must be as close to the cutter head as possible to require a minimum force to swing the pontoon back and forth. On the contrary, the side wire must be kept as far away as possible to prevent the wire getting tangled in the cutter head.

2.3 Side wire anchoring

The back and forth swinging motion of the cutter head dredger around the working spud is achieved by hauling and veering the side wires connected to the anchors. The anchors are positioned with a certain offset along the pontoon's center line and a certain distance forward of the spud position. As a rule of thumb, the holding force is estimated by multiplying a factor by the weight of the anchor. The factor is dependent on the type of anchor. The type of anchor is dependent on the rock to be excavated and the expected anchor forces. An anchor that is too light will break out prematurely, while an anchor that is too heavy will damage auxiliary equipment.

The (re)positioning of the anchors is a comprehensive activity. This can be done using the anchor booms of the cutter suction dredger or auxiliary equipment as a multicat[1]. The anchors are positioned at a fairly great distance from the cutter suction dredger to increase the operation time before the next shift. A greater distance mostly implies a better equalizing of the forces on both wires (starboard and port side). The anchor positions make an angle relative to the cutter head, which determines what part of the excavation force must be counteracted. A disadvantage of the great distance is the elasticity of the side wires. The deployed anchors are visualized in figure 2.4.

[1]A multicat is a small self propelled vessel to execute support jobs at sea in function of a larger construction vessel

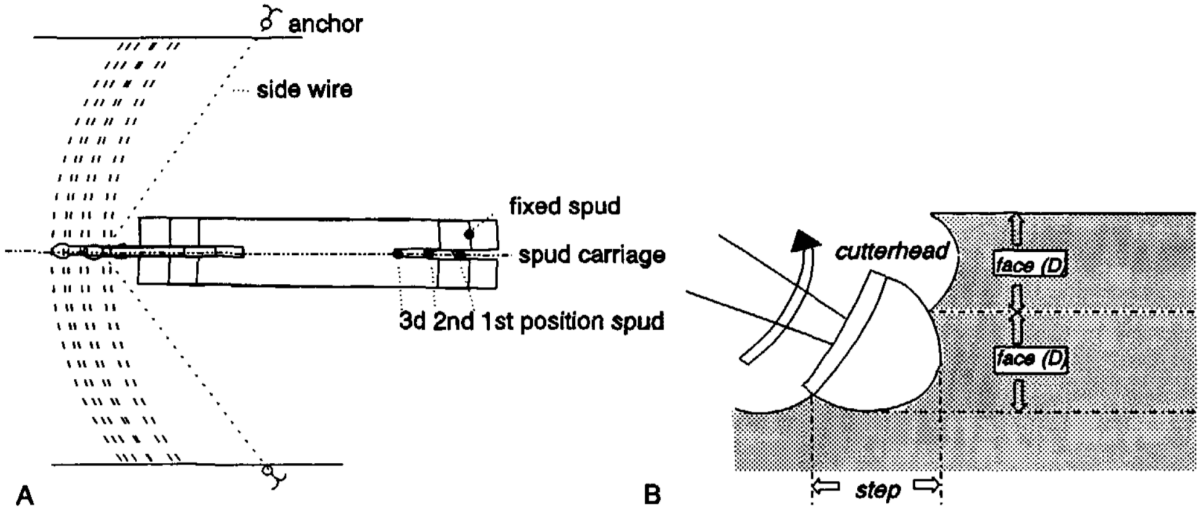

Figure 2.4: The spud and anchoring system of a cutter suction dredger (Verhoef (1997))

2.4 Spud system

The spud system has multiple purposes. The spud system is able to make a step motion, act as a rotation point for the swing motion and counteract the longitudinal forces originating from the excavation process. In hard to very hard rock types, the spud will not penetrate the seabed very deep. The maximum longitudinal force that a spud can carry is therefore still a roughly estimated parameter. The step motion can theoretically be performed anywhere along the bank cut, but in the corner of a swing gives the most regular cut pattern.

In figure 2.4, the spud working principle is visualized. The pontoon is shifted whereby the spud position relative to the pontoon is changing.

2.5 The cutter head drive

Two types of cutter head drive are currently in use: electric or hydraulic. It is common practice to position the cutter head drive at the end of the ladder, near the hinge point. In some cases a drive in a watertight housing is positioned under water closer to the cutter head, with a reduced length of the cutter head shaft as a consequence. A cutter head shaft connects the drive output shaft with the cutter head. A gearbox is positioned in between to transform the high rotational speed of the drive to the required rotational speed of the cutter head.

In this thesis, an electric drive is considered positioned near the hinge point. No other types and positioning of cutter head drives are further discussed. In this particular case, the cutter head drive train is a long, vibration sensitive part of the cutter suction dredger.

2.5.1 Inertia effect

When describing the inertia effect of the cutter drive, an irregular cutting process is considered. Such a cutting process can be found in hard to very hard rock types, which are the rock types considered in this thesis. Inertia can be favorable during an irregular cutting process. Rotational energy is stored in the fast turning electric drive and the flywheel effect absorbs all the peak loads. Nevertheless the drive shaft and gearbox are charged with these fluctuating loads.

The fluctuating loads on the cutter head shaft and gearbox may initiate vibration problems when the load frequency is near the natural frequency of the entire cutter head drive. Resonance phenomena and

torsion oscillations may occur when small periodic loads have the ability to store vibration energy and produce large amplitude oscillations. A drastic reduction in service life or failure of the gearbox and/or shaft can be a consequence of resonance effects.

When measuring torque on the cutter head shaft (in front of the gearbox and drive), positive and negative torque values alternate each other due to the highly irregular cutting process. During the breakout of a large piece of rock, torque is built up by reducing the cutter head circumferential velocity. When the rock part is cut loose, the cutter head circumferential velocity is built up again. The rock being excavated counteracts the rotational motion of the cutter shaft introduced by the cutter head drive. When this counteracting force is not continuously present, a torsional vibration is introduced. These torsional vibrations cause hammering in the gearbox.

2.5.2 Drive characteristics

The pontoon rotates around the working spud by side winches which haul or veer wires connected to the anchors. By pulling the cutter head against the uncut rock, the cutter drive load is kept as high as possible. It is inevitable that the maximum available cutter drive torque will be exceeded during the fluctuating loads. The drive has to handle these temporary overloads by balancing between circumferential velocity and drive torque. The relationship between both output parameters is given in the drive characteristic.

The drive characteristic is a graph relating torque and circumferential speed. The circumferential speed is given on the vertical axis and the torque on the horizontal axis. A constant power line along which the drive can operate is shown (see figure 2.5). Electric drives can deliver torque overloads. The maximum torque is often around 150 percent of its nominal value. The torque restriction line shows the decreasing circumferential velocity in function of the torque overload. This overload zone is of high importance during an irregular cutting process. A cutter head drive can handle a torque overload during a short period, but stalling of the cutter head must be prevented. The steady state operation zone of an electric drive is also visualized in figure 2.5.

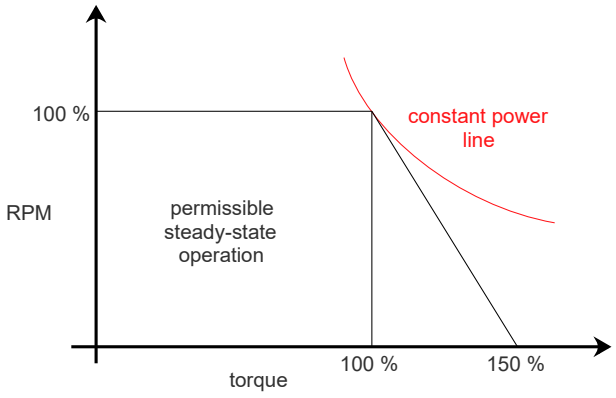

Figure 2.5: Torque-RPM graph of an electric drive

2.6 Hull characteristics

The hull characteristics define the swing width of a cutter suction dredger. All equipment discussed in the previous paragraphs is positioned somewhere on the hull. The most important parameters are the position of the working spud and hinge point of the ladder. The swing radius of the cutter suction dredger equals the distance between the cutter head and the working spud. To excavate big cuts, a swing radius as large as possible is required. The general lay-out of a mega cutter suction dredger is shown in figure 2.6.

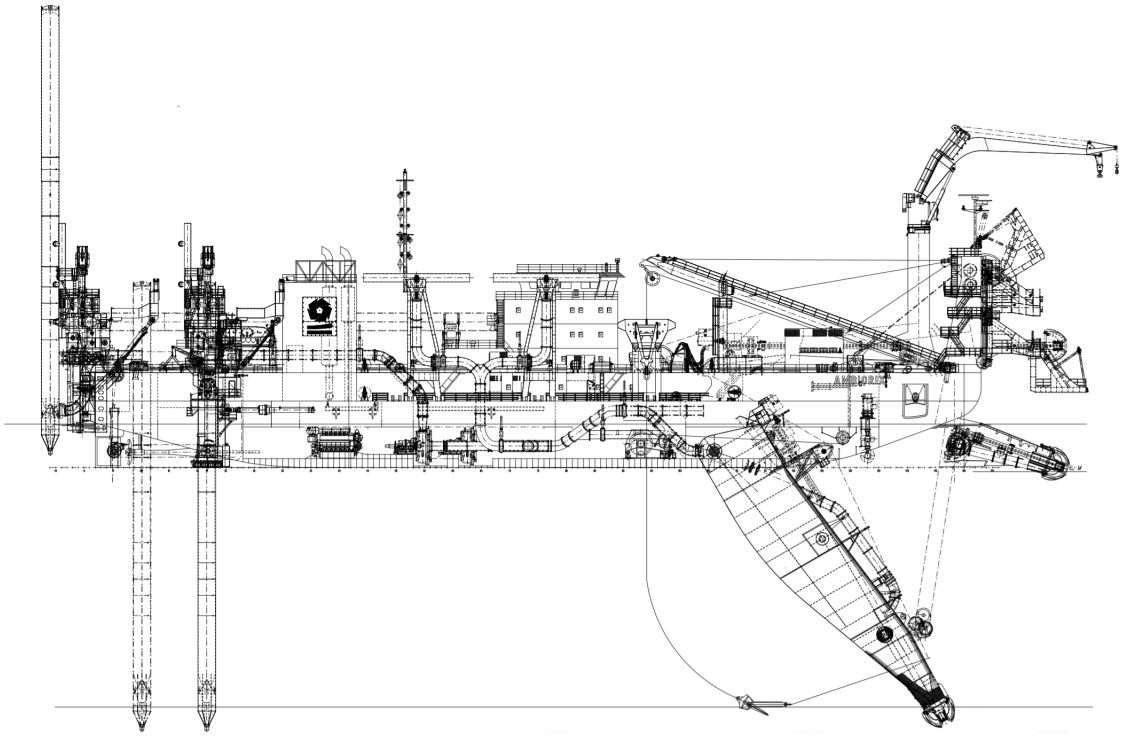

Figure 2.6: The general lay-out of the Ambiorix

Chapter 3

Geometry and kinematics of a cutter head

The simulation of the cutting process requires a good understanding of the geometry of a cutter suction dredger. The goal of the geometric model is to simulate a moving cutter head in space and time. The geometry will be discussed in the first part of this chapter, the kinematics will follow in the second part.

The geometric part describes the coordinate systems used to define a cutter head and its motions. The coordinate systems describe the cutter suction dredger from tooth to spud in their corresponding reference frame. The next part of this chapter describes the motions that are imposed on the cutter head (swing motion, circumferential motion and step). The kinematics (position, velocity and path) of a cutting tooth are discussed in the last part of this chapter.

3.1 Coordinate systems and geometry

A cutter suction dredger has a complex geometry. Using 3D-CAD drawings to model the cutter suction dredger would be time consuming and worthless whereas the modeling of the cutter head-rock interaction only requires discrete modeling of the pontoon, cutter head contour and teeth parameters. The simplification of shapes that are used to define the cutting teeth, cutter head and pontoon are explained together with the coordinate systems required to describe and correlate them.

A cutter suction dredger relative to the surrounding rock is defined in the earth coordinate system. The ladder motion is defined in the pontoon coordinate system. The tooth positions and orientations are defined in the cutter head coordinate system. The cutter head, pontoon and earth coordinate systems are visualized in figure 3.1 to give a general overview of the reference frames used. The parameters visualized in this figure are discussed in sections 3.1.1 and 3.1.2. The tooth coordinate system is visualized in section 3.1.4. Because of the substitutability and abradability of a tooth, an adapter coordinate system is introduced to make a tooth replaceable. This adapter coordinates system allows to switch between different tooth types on the same type of cutter head, which makes it possible to investigate the influence of a specific tooth type.

3.1.1 Earth coordinate system

To model the cutter head-rock interaction, a fixed general reference frame is required to describe the motions and presence of objects in a three-dimensional space. The earth coordinate system serves as the general reference frame and is visualized in figure 3.1.

Two reference points are indicated in figure 3.1: the hinge point (H) and the suction inlet point (I). The hinge is the point of rotation of the cutter ladder and the suction inlet point is the entry of the suction pipeline. Both points are indicated in figure 3.1 with coordinates h_1, h_2, h_3 (hinge point) and i_1, i_2, i_3

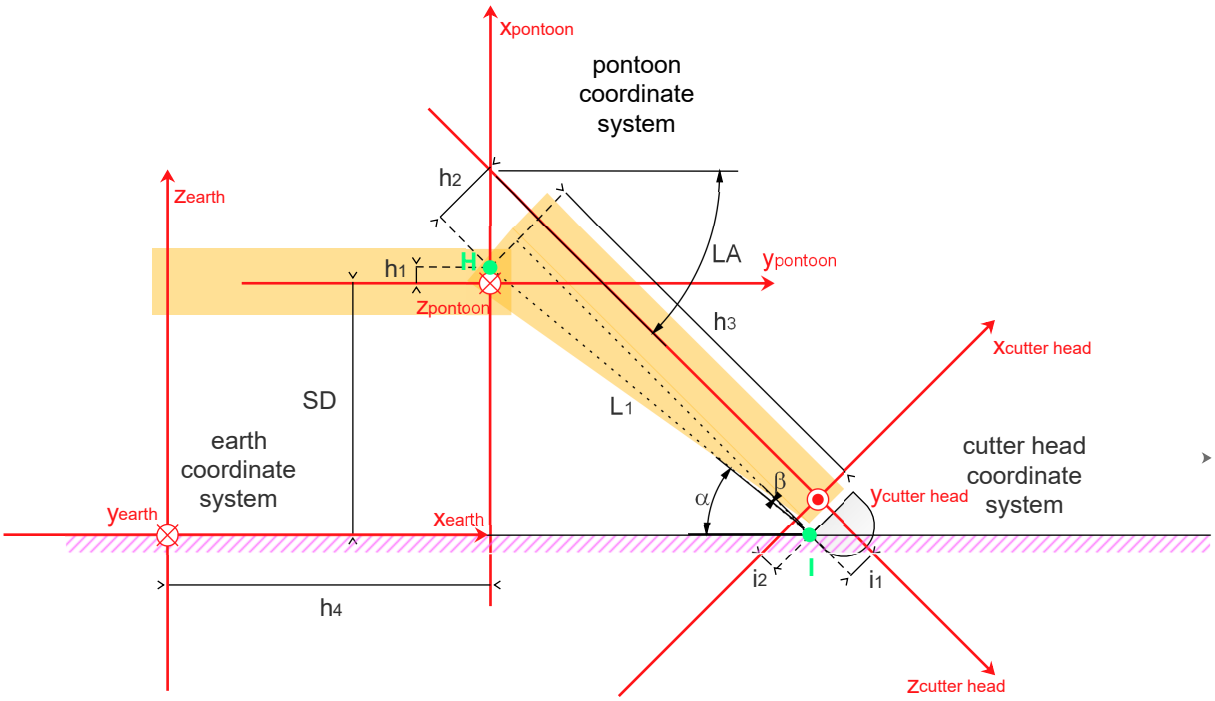

Figure 3.1: Coordinate systems required to define a cutter suction dredger

(suction inlet). The position of the suction inlet is used to calculate the suction depth or dredged depth of the cutter head. These two reference points are important to correlate each of the reference frames. The origin and axes of the earth coordinate system are defined as follows:

O_{earth}: the spud position vertically shifted down or up till the seabed

x_{earth}: parallel with the waterline on the seabed, longitudinal, positive to the cutter head

y_{earth}: parallel with the waterline at the seabed, transversal, positive to port side of the pontoon

z_{earth}: perpendicular to the waterline and through the working spud, positive to the upper part of the pontoon

This coordinate system is fixed and locates the cutter suction dredger in the surrounding rock. The hinge-spud distance (h_4), suction depth (SD) and hinge to water line distance (h_1) are required to define the pontoon coordinate system relative to the earth coordinate system. These parameters are visualized in figure 3.1.

3.1.2 Pontoon coordinate system

The pontoon coordinate system is visualized in figure 3.1. The aim of the pontoon coordinate system is to define the ladder position (rotation around the hinge) relative to the pontoon. The ladder angle is the sum of angles α and β in figure 3.1.

The pontoon coordinate system with its reference points (H and I) makes it possible to define a suction depth (SD) or ladder angle (LA). Either the suction depth or ladder angle is required to calculate further dredging parameters (f.e. swing radius, position of the cutter head relative to the pontoon). Two different ladder angles are shown in figure 3.2. If the suction depth is given as input parameter, the corresponding ladder angle is obtained. Each cutter suction dredger has limited capacities concerning the suction depth and corresponding ladder angle. A maximum value is obtained using the parameters h_1, h_2, h_3 and the cutter head contour. The origin and axes of the cutter head coordinate system are defined as follows:

$O_{pontoon}$: the hinge position vertically shifted down till the waterline

$x_{pontoon}$: perpendicular to the waterline and through the symmetry axis of the ladder hinge, positive to the upper part of the pontoon

$y_{pontoon}$: on the water line, longitudinal, positive towards the cutter head

$z_{pontoon}$: parallel with the waterline, transverse, positive to port side of the pontoon

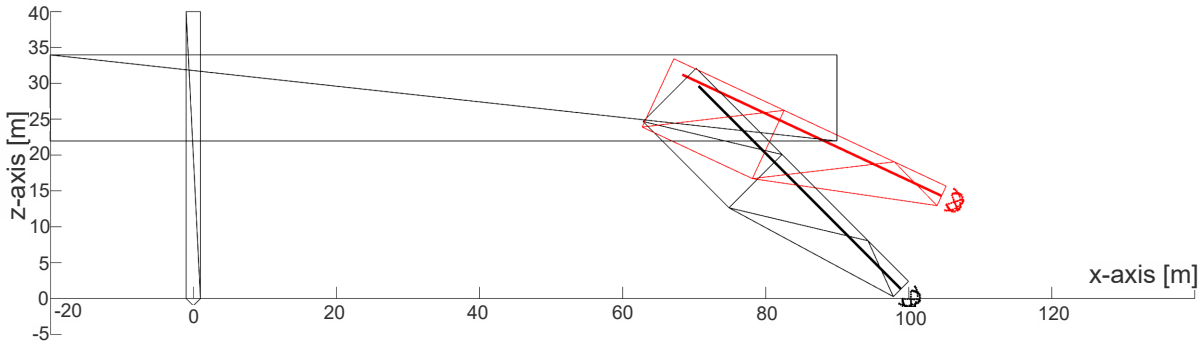

Figure 3.2: Two different ladder angles (25° (red) and 45° (black)) in the earth coordinate system

3.1.3 Cutter head coordinate system

To describe the position of a cutting tooth, the cutter head coordinate system is set up. The cutter head coordinate system is visualized in figure 3.3. Three parameters are required to define the position of a cutting tooth on the cutter head. The tooth tip is defined as the tooth position. For each tooth, a vertical coordinate defines the position along the cutter head axis starting from the cutter head back ring (z-direction). A radial coordinate defines the radial position of the tooth from the cutter head axis (radial distance to z-axis). The third coordinate is the sweep angle which describes the angle around the cutter head axis relative to the first tooth. This angle is measured counter clockwise around the z-axis starting from the x-axis.

$O_{cutter\ head}$: bottom of back ring, center of cutter head circular contour

$x_{cutter\ head}$: perpendicular to the cutter head axis, through tooth tip number one

$y_{cutter\ head}$: perpendicular to the cutter head axis and x-axis

$z_{cutter\ head}$: cutter head axis, positive towards the upper part of the cutter head

The magenta colored tooth (on the positive x-axis, see figure 3.3) is tooth number one. The sweep angle of all other teeth is defined relative to this tooth, which sweep angle is set to 0. The coordinates of all teeth are obtained from the manufacturer of the cutter head and are corresponding a specific tooth type. The model built in this research will correct the tooth position depending on the tooth type mounted on the cutter head.

3.1.4 Tooth coordinate system

To describe the orientation of a cutting tooth, the cutting tooth coordinate system is created. Three parameters are required to define the orientation of a cutting tooth on a cutter head. The definition of the tooth orientation depends on the brand of the tooth and cutter head. The VOSTA[1]-definition serves as a reference frame within this research. Other definitions are first converted to this VOSTA-definition

[1]VOSTA LMG is a manufacturer of dredging equipment, http://www.vostalmg.com

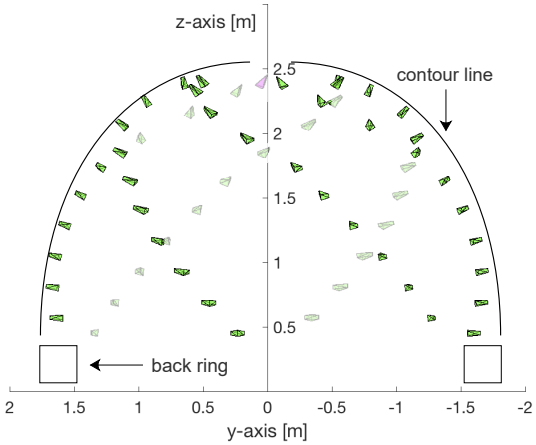

(a) Side view, YZ-plane

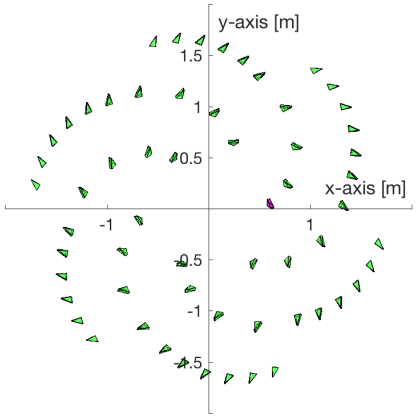

(b) Top view, XY-plane

Figure 3.3: Cutter head coordinate system

before implementation.

The orientation of a VOSTA-tooth is defined by three angles: the cutting, contour and root angle. A tooth can obtain a certain orientation by incorporating an offset angle in the tooth design and/or by orientating the tooth in the adapter on the cutter head. The cutting angle is largely incorporated in the tooth design and partly dependent on the adapter orientation.

A simplified tooth within the tooth coordinate system is visualized in figure 3.4. The coordinate system's origin and axes are described as follows:

O_{tooth}: tooth tip, center cutting edge

x_{tooth}: negative tooth axis, in the cutting plane

y_{tooth}: through the tooth tip and perpendicular to the tooth axis and leading edge, positive towards the adapter connection

z_{tooth}: leading edge axis

A cutting tooth has a complex design to withstand the cutting forces and obtain an optimal wear profile during the excavation process. A simplified tooth is built to model the process with minimal computational time, whereby only the abradable part is constructed. The purpose of the other part of the cutting tooth is of no value during this research. Five parameters define the shape of this simplified tooth:

- backward angle [mm], see figure 3.4b
- lateral angle [deg], see figure 3.4d
- leading edge [mm], see figure 3.4d
- wear length [mm], see figure 3.4b

Figure 3.4 visualizes the simplified tooth shape. A three-dimensional view gives a general impression of the shape, whereafter each of the aspects is shown. The cutting face (Dutch: spaanvlak) is indicated in figure 3.4b. This is the area which will be in contact with rock during the transport of excavated material.

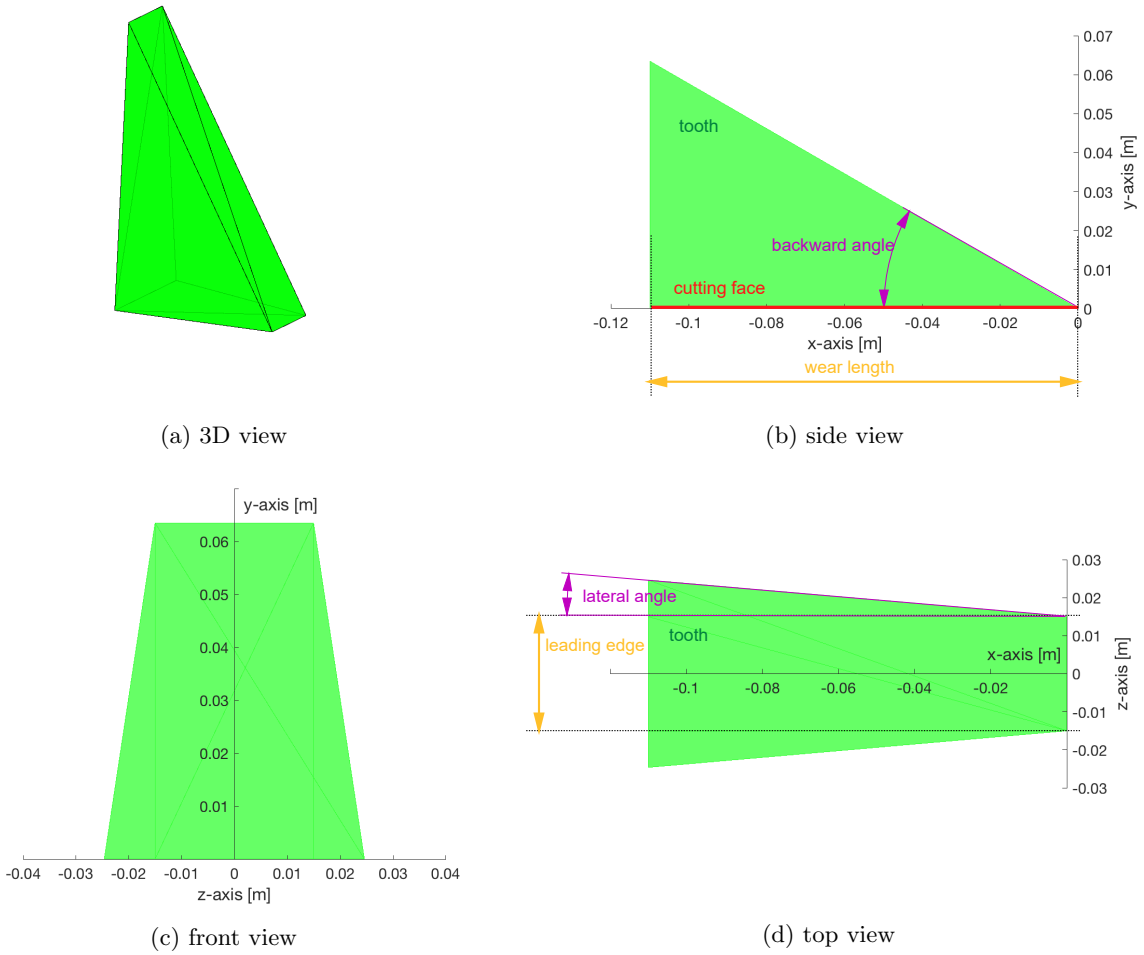

(a) 3D view

(b) side view

(c) front view

(d) top view

Figure 3.4: simplification of a cutting tooth

While executing geometric simulations of a cutter head, the teeth must be interchangeable because different tooth types can be used on the same type of cutter head. A tooth is locked in an adapter. The adapter end of a tooth has standard dimensions, which are identical for all tooth types. For this reason the origin of the adapter coordinate system is positioned at the end of the abradable part of a tooth, which is a fixed point on the adapter. Depending on the tooth type, the abradable part can differ in

orientation and shape. The model converts the tooth tip positions for different tooth types. This allows the software to investigate the influence of the tooth type on the excavation process.

The wear process of a cutting tooth is modeled by correcting the tooth tip position and tooth shape. A non worn tooth is shown in figure 3.4. The worn shape is created by reducing the wear length. A vertical line in the XY-plane defines the new tooth tip and corresponding wear area.

3.2 Motions

3.2.1 Step motion

The step size is a parameter defined by the dredge operator. The cutter suction dredger is shifted forward, while the working spud is kept in position. This shift increases the distance between the working spud and the cutter head by the step size, thus a bigger swing radius is obtained. The step motion in the model is applied in the earth coordinate system as a fictive increase of pontoon length.

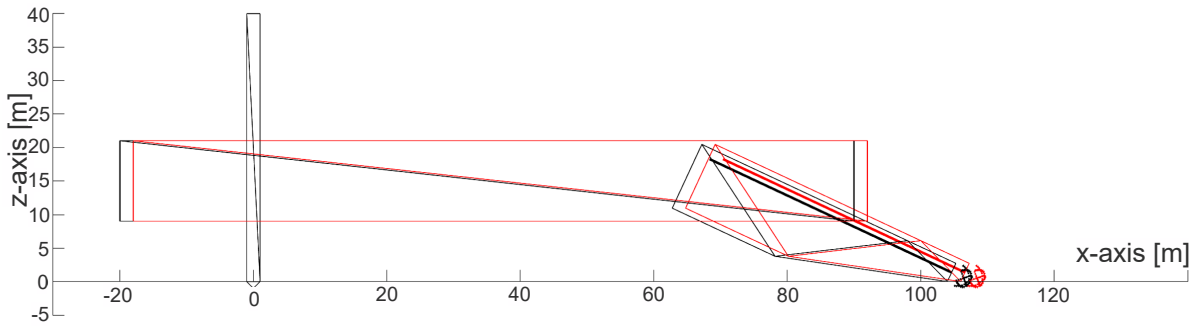

Figure 3.5: Step motion of a cutter head

The model first checks for the maximum ladder angle. After this parameter is validated against the maximum value, the maximum step size is calculated. The user-defined step size is then validated against the maximum step size.

3.2.2 Swing motion

The swing motion is a circumferential motion around the working spud. This motion is modeled in the earth coordinate system. A maximum swing angle is required to give an offset ($\theta_{\text{offset,ch}}$) for the cutter suction dredger (black plots in figure 3.6) and defines the width of the bank cut. The zero-position is reached when the cutter head axis coincides with the positive x-axis of the earth coordinate system (red plot in figure 3.6). The swing motion of the cutter head around the working spud is determined by an angular velocity (ω_{swing}) in the earth coordinate system around the z-axis. The position of the cutter head while swinging is modeled as in equation 3.1. θ_{ch} is measured positively counter clockwise around the z-axis.

$$\theta_{\text{ch}} = \theta_{\text{offset,ch}} + \omega_{\text{swing}} \cdot \text{t} \tag{3.1}$$

where:

θ_{ch} = angular position cutter head in earth coordinate system [rad]

$\theta_{\text{offset,ch}}$ = angular begin position in earth coordinate system [rad]

ω_{swing} = angular velocity around z-axis in earth coordinate system [rad/s]

t = time elapsed [s]

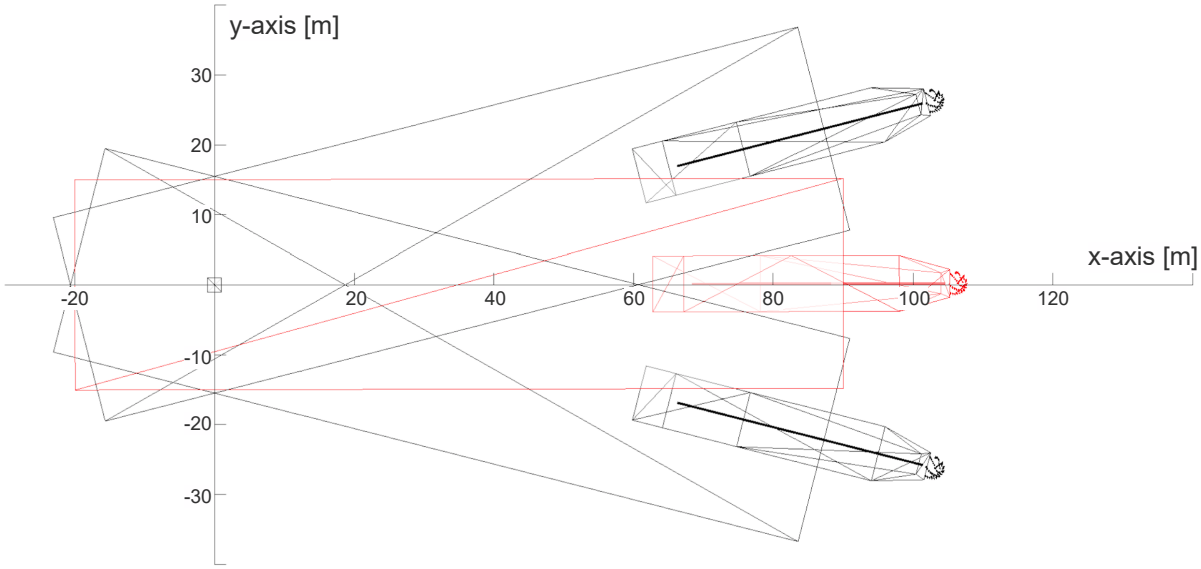

Figure 3.6: Swing motion of a cutter head

3.2.3 Circumferential motion

The cutter head is driven by the cutter shaft which introduces a circumferential motion. Each tooth starts the circumferential motion with an initial offset (θ_{sweep}) from the zero-position. This zero-position is reached when the tooth tip is laying on the positive x-axis (magenta tooth in figure 3.3). The circumferential motion of the cutting tooth around the cutter head axis is determined by an angular velocity (ω_{circ}) in the cutter head coordinate system (around the z-axis). The circumferential motion is modeled by equation 3.2.

$$\theta_{\text{t}} = \theta_{\text{sweep}} + \omega_{\text{circ}} \cdot \text{t} \tag{3.2}$$

where:

θ_{t} = angular position tooth in cutter head coordinate system [rad]

θ_{sweep} = initial sweep angle of tooth in cutter head coordinate system [rad]

ω_{circ} = angular velocity around z-axis in cutter head coordinate system [rad/s]

t = time elapsed [s]

3.3 The coordinate system transformations

To define all positions, orientations, shapes and movements of the teeth on the cutter head in the rock matrix coordinate system[2], a definition was necessary to describe the link between the different reference frames. To do so, the Denavit-Hartenberg (D-H) convention, known from robotics applications, is applied to the cutter suction dredger in general. The advantage of using the D-H convention is the simplification and standardization of the kinematic analysis for systems connected with linkages. Some general definitions and agreements have to be applied, which are discussed in this section.

Using the D-H convention, a structure (cutter suction dredger) is subdivided in joints and links, where joints connect the links. Joints can be actuated, causing the links to move. There are n joints and (n-1)

[2]The rock matrix coordinate system is a a reference frame which coincides with the modeled rock mass surrounding the cutter head working area, chapter 4 section 4.7.2.

links in a structure. The cutter suction dredger is subdivided in 7 joints (0-6) and 6 links (0-5). The 7 joints and 6 links are indicated in figure 3.7. The earth coordinate system coincides with joint 1, the pontoon coordinate system coincides with joint 3, the cutter head coordinate system coincides with joint 5 and tooth coordinate system coincides with joint 6. Coordinate system 0 (base frame) coincides with the rock matrix coordinate system, which is further explained in chapter 4, section 4.7.2.

The naming convention used in figure 3.7 means that actuating joint i leads to a movement of link i. The cutter suction dredger in figure 3.7 contains revolute and prismatic joints. A revolute joint rotates around a single axis, a prismatic joint translates along a single axis. Joint 2 is a prismatic joint, because the degree of freedom is a translation along the z-axis. All other joints are revolute and can rotate about their z-axis. The D-H convention requires that the axis of actuation for joint (i+1) is z_i. To set up all coordinate systems, the following assumptions must be met:

- the axis x_i is perpendicular to z_{i-1}
- the axis x_i intersects z_{i-1}

3.3.1 Locate and label the joint axes

First step in setting up a sketch for D-H parameterisation is locating and labeling the joint axes. For a cutter suction dredger, this implicates the introduction of 7 joint axes z_0 till z_6. The axis z_0 is called the base axis, forming part of the base frame, but not able to be actuated. Each joint axis simulates a specific function of the cutter suction dredger. In figure 3.7, the joint axes are always the longitudinal cylinder axes (black cylinders at each joint).

z_1: rotation of the pontoon around the spud

z_2: translation of the spud carriage

z_3: rotation of ladder around the hinge

z_4: rotation of the cutter head around cutter head axis

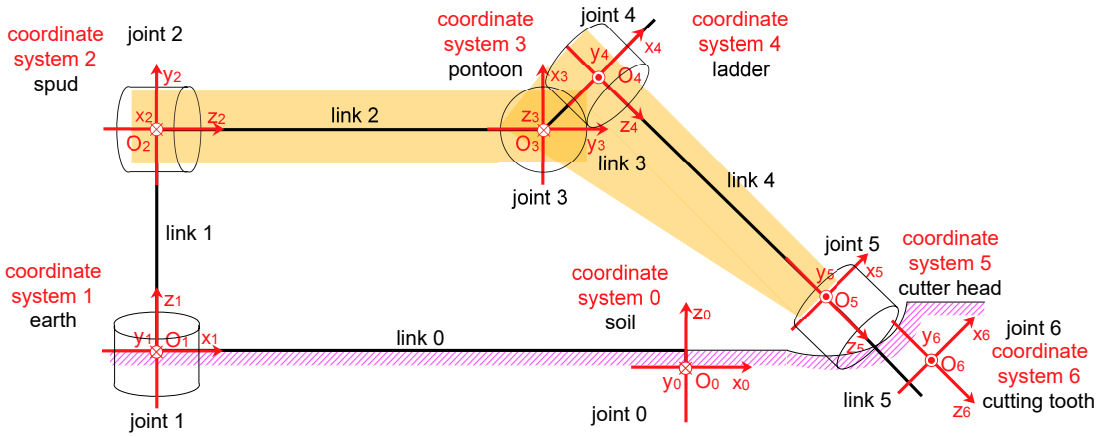

Figure 3.7: Each link fitted with a coordinate system

3.3.2 Computing the link parameters

The D-H convention uses four parameters to describe the position and orientation of two adjacent coordinate systems. These parameters are described as follows:

a_i: translation along x_i from O_i to the intersection of x_i and z_{i-1}

d_i: translation along z_{i-1} from O_{i-1} to the intersection of x_i and z_{i-1}

β_i: angle from z_{i-1} till z_i around x_i

θ_i: angle from x_{i-1} till x_i around z_{i-1}

a_i is measured positively in the direction of axis x_i. d_i is measured positively in the direction of axis z_{i-1}. β and θ are measured positively counter clockwise, following the right hand rule.

3.3.3 Defining the joint variable

To describe the state of each joint, a joint variable must be defined. For a revolute joint the current angle of rotation and for a prismatic joint the position along the axis of translation, will be described in this variable. Each joint has only one variable. The notation is as follows:

$$q_i = \begin{cases} \theta_i & \text{if joint } i \text{ is revolute} \\ d_i & \text{if joint } i \text{ is prismatic} \end{cases}$$

3.3.4 General transformation matrix

Each link is fitted with a coordinate system (figure 3.7). In this way, every point on link i can be described and is fixed to coordinate system i. The 7 coordinate systems are linked to each other using the Denavit-Hartenberg parameters. The four Denavit-Hartenberg parameters describe the link between each of these reference frames.

To express the position and orientation of an arbitrary point O_i, x_i, y_i, z_i with respect to a point in adjacent coordinate system $O_{i-1}, x_{i-1}, y_{i-1}, z_{i-1}$, a homogeneous transformation matrix A is required. This matrix will be a combination of translations and rotations. While each joint moves, each transformation matrix will change but stays only dependent on one joint variable q_i.

To express the position and orientation of O_j, x_j, y_j, z_j with respect to O_i, x_i, y_i, z_i, a transformation matrix M is required. This matrix M will be defined as follows:

$$M_j^i = \begin{cases} A_i \cdot A_{i+1} \cdot ... \cdot A_{j-1} \cdot A_j & \text{if } i < j \\ I & \text{if } i = j \\ (M_j^i)^{-1} = M_i^j & \text{if } i > j \end{cases}$$

In this way, a complicated transformation is broke up in several consecutive transformations and it is possible to transform coordinates between the tooth (CS6) and rock matrix coordinate system (CS0). Using the D-H convention, homogeneous matrix A can be split up in four basic transformations:

$$A_i = R(z, \theta_i) \cdot T(z, d_i) \cdot T(x, a_i) \cdot R(x, \beta_i) \tag{3.3}$$

These transformations are defined as follows:

R(z, θ_i): rotation around z-axis by θ_i

T(z, d_i): translation along z-axis by distance d_i

T(x, a_i): translation along x-axis by distance a_i

R(x, β_i): rotation around x-axis by β_i

In matrix formulation:

$$
\begin{aligned}
\mathrm{R(z,\theta_i)} &= \begin{bmatrix} \cos\theta_i & -\sin\theta_i & 0 & 0 \\ \sin\theta_i & \cos\theta_i & 0 & 0 \\ 0 & 0 & 1 & 0 \\ 0 & 0 & 0 & 1 \end{bmatrix} \\
\mathrm{T(z,d_i)} &= \begin{bmatrix} 1 & 0 & 0 & 0 \\ 0 & 1 & 0 & 0 \\ 0 & 0 & 1 & d_i \\ 0 & 0 & 0 & 1 \end{bmatrix} \\
\mathrm{T(x,a_i)} &= \begin{bmatrix} 1 & 0 & 0 & a_i \\ 0 & 1 & 0 & 0 \\ 0 & 0 & 1 & 0 \\ 0 & 0 & 0 & 1 \end{bmatrix} \\
\mathrm{R(x,\beta_i)} &= \begin{bmatrix} 1 & 0 & 0 & 0 \\ 0 & \cos\beta_i & -\sin\beta_i & 0 \\ 0 & \sin\beta_i & \cos\beta_i & 0 \\ 0 & 0 & 0 & 1 \end{bmatrix}
\end{aligned}
\tag{3.4}
$$

$$
\mathrm{A_i} = \begin{bmatrix} \cos\theta_i & -\sin\theta_i\cos\beta_i & \sin\theta_i\sin\beta_i & \mathrm{a_i}\cos\theta_i \\ \sin\theta_i & \cos\theta_i\cos\beta_i & -\cos\theta_i\sin\beta_i & a_i\sin\theta_i \\ 0 & \sin\beta_i & \cos\beta_i & \mathrm{d_i} \\ 0 & 0 & 0 & 1 \end{bmatrix} \tag{3.5}
$$

Joints 1, 3 and 5 in figure 3.7 are revolute causing parameter θ_i to vary. Joint 2 is prismatic causing parameter $\mathrm{d_i}$ to vary.

The output of the geometrical transformations are the tooth shape, position and orientation in the rock matrix coordinate system. In the discrete model, these parameters are calculated during each time step for each tooth. All positions are transformed by equation 3.6.

$$
\mathrm{P_i} = \mathrm{M_j^i} \cdot \mathrm{P_j} \tag{3.6}
$$

3.4 Kinematics of a cutting tooth

To predict the forces generated by the movement of a cutter head, the kinematics of a single tooth must be well understood. After modeling the positioning of a cutting tooth in space and time, this chapter will deal with the kinematic behavior of a single tooth.

The physical parameters which determine the cutting process of a tooth in rock will be discussed in this chapter. The motion of a cutting tooth will be investigated in the plane perpendicular to the cutter head axis. A right turning cutter head is observed.

3.4.1 The path of a tooth tip

The path of a single tooth tip is shown in figure 3.8. A front view of the cutter head is used to explain the orthocycloid path of a tooth tip. In figure 3.8, two circles are shown. These circles represent the lowest and highest tooth positions. Circle C is unrolled and the periphery forms line k. The cutter head moves sideways with the swing velocity v_{swing} (m/s) and rotates with the angular velocity ω_{circ} (rad/s). Point P is the pole of the orthocycloid. The pole is the position where the horizontal velocity of a tooth tip is zero and changes direction. Point A(0) is a random tooth tip at t = 0.

The swing velocity as well as the circumferential velocity can obtain positive and negative values. In this research, the circumferential velocity is assumed to be negative (left turning cutter head). A combination of both values can trigger two possible ways of dredging: over- and undercutting. During overcutting, the bank is approached by the cutting teeth from above. During undercutting, the bank is approached from below. At the end of a full swing, the swing direction is reversed and the cutter head switches from under- to overcutting or vice versa.

All teeth are divided over several blades. The tooth positions on a blade can differ compared to the previous and next blade (staggered). The staggering is expressed in the number n, which indicates how much blades are in between two similar tooth positions with the same vertical height above the back ring and radial distance from the cutter head axis. Depending on the staggering (n) and amount of blades (m), the amount of teeth on one contour circle (p) is changing. Equation 3.7 calculates how many tooth tips are located at each contour line. Each tooth tip is $\frac{2 \cdot \pi}{p}$ radians away from each other.

$$p = \frac{m}{n} \tag{3.7}$$

When the swing velocity is reduced till zero, the motion of a tooth tip simplifies from a orthocycloid to a circle. Equation 3.8 is valid for an overcutting cutter head. In this case, the pole of each tooth tip lays on the negative z-axis. During undercutting, the sign of the swing velocity changes and equation 3.9 is valid. During undercutting, the pole of each tooth tip is somewhere along the positive z-axis. At the end of a full swing, the sign of the pole's x-value is changed.

For overcutting:

$$\begin{aligned} y &= v_{swing} \cdot t + R \cdot \sin(\theta_{sweep} + \omega_{circ} \cdot t) \\ x &= R \cdot \cos(\theta_{sweep} + \omega_{circ} \cdot t) \end{aligned} \tag{3.8}$$

For undercutting:

$$\begin{aligned} y &= -v_{swing} \cdot t + R \cdot \sin(\theta_{sweep} + \omega_{circ} \cdot t) \\ x &= R \cdot \cos(\theta_{sweep} + \omega_{circ} \cdot t) \end{aligned} \tag{3.9}$$

3.4.2 Velocity of a tooth tip

The velocity of a tooth tip is the derivative with respect to time of the position. It is combination of a circumferential velocity around the cutter shaft and around the working spud.

$$\begin{aligned} \frac{dy}{dt} &= v_y = v_{swing} + R \cdot \omega_{circ} \cdot \cos(\theta_{sweep} + \omega_{circ} \cdot t) \\ \frac{dx}{dt} &= v_x = -R \cdot \omega_{circ} \cdot \sin(\theta_{sweep} + \omega_{circ} \cdot t) \end{aligned} \tag{3.10}$$

The total cutting velocity is the sum of the y- and z-vector.

$$v_{cut} = \sqrt{v_x^2 + v_y^2} \tag{3.11}$$

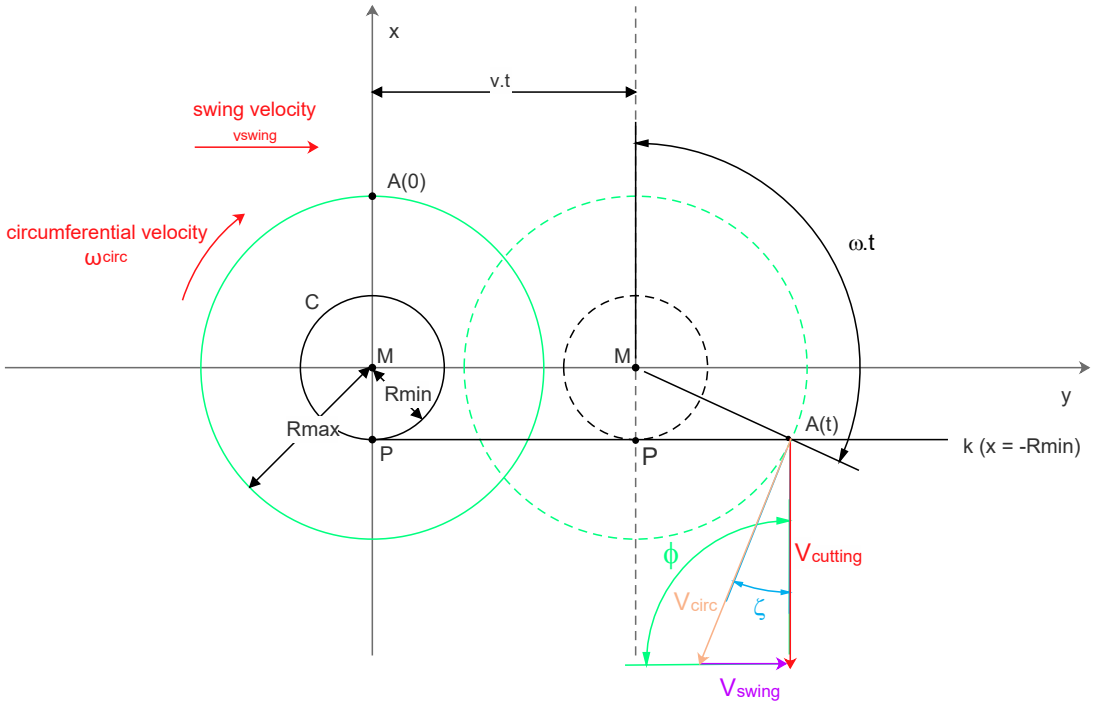

Figure 3.8: Definitions of the orthocycloid path of a tooth tip

For overcutting, the total velocity v_{over} equals:

$$\mathrm{v_{over}} = \sqrt{\mathrm{v_{swing}^2} + 2 \cdot \mathrm{v_{swing}} \cdot \mathrm{R} \cdot \omega_{\mathrm{circ}} \cdot \cos(\theta_{\mathrm{sweep}} + \omega_{\mathrm{circ}} \cdot \mathrm{t}) + \mathrm{R}^2 \cdot \omega_{\mathrm{circ}}^2} \tag{3.12}$$

For undercutting, the total velocity v_{under} equals:

$$\mathrm{v_{under}} = \sqrt{\mathrm{v_{swing}^2} - 2 \cdot \mathrm{v_{swing}} \cdot \mathrm{R} \cdot \omega_{\mathrm{circ}} \cdot \cos(\theta_{\mathrm{sweep}} + \omega_{\mathrm{circ}} \cdot \mathrm{t}) + \mathrm{R}^2 \cdot \omega_{\mathrm{circ}}^2} \tag{3.13}$$

The Denavit-Hartenberg convention (D-H convention, see section 3.3) is used to calculate the velocity direction of a cutting tooth in the rock matrix coordinate system. The importance of the velocity direction will become clear in chapters 4 during the application of the cutting models. The D-H convention is an optimal method to transform the velocity vectors in space. By using the transformation matrix defined in section 3.3 and setting up a velocity matrix W, it is possible to transform the velocity vectors in space. The velocity matrix W is defined in equation 3.14. In this matrix, the angular or translational velocities in a reference frame j are expressed.

$$\mathrm{W_j} = \begin{bmatrix} 0 & -\omega_z & \omega_y & v_x \\ \omega_z & 0 & -\omega_x & v_y \\ -\omega_y & \omega_x & 0 & v_z \\ 0 & 0 & 0 & 0 \end{bmatrix} \tag{3.14}$$

To transform the velocity matrix within reference frame j relative to reference frame i, the D-H convention is characterized by the transformation rule in equation 3.15.

$$\mathrm{W_i} = \mathrm{M_j^i} \cdot \mathrm{W_j} \cdot \mathrm{M_i^j} \tag{3.15}$$

This velocity matrix is calculated for the swing motion around the working spud as well as the circumferential motion around the cutter shaft. Both velocity matrices are add up (equation 3.16) to create the cutting velocity matrix.

$$W_i = W_{i,swing} + W_{i,circ} \tag{3.16}$$

To finally calculate the cutting velocity vector $\vec{V}_{cut}$ with respect to reference frame i (rock matrix coordinate system), the tooth position (P_i) is multiplied by the velocity matrix W_i (equation 3.17).

$$\vec{V}_{cut} = W_i \cdot \vec{P}_i \tag{3.17}$$

3.4.3 Cutting phase of a tooth tip

During the rotation and swing motion of a cutter head, a tooth runs through a cutting phase and a non-cutting phase. Depending on the step length and face height, this varies for each tooth position. During the excavation of an intact rock mass, no breaching processes[3] occur. This implies that all the rock material must be excavated before it can be picked up by the suction pipe. The bank of rock in front of the cutter head will take the shape of the cutter head contour. During the excavation of a very weathered rock mass, breaching may become a dominant factor. This situation will not be further discussed in this research.

The shape of the face is visualized in figure 3.9. The shape of the bank during the first cut is indicated by the yellow line. The shape of the bank during the next cut, after stepping forward, is shown by the red line. The dotted lines indicate the tooth positions of the stepped cutter head where a different cutting phase is encountered. During the modeling of the cutter head in this research, this cutting phase is calculated during every time step.

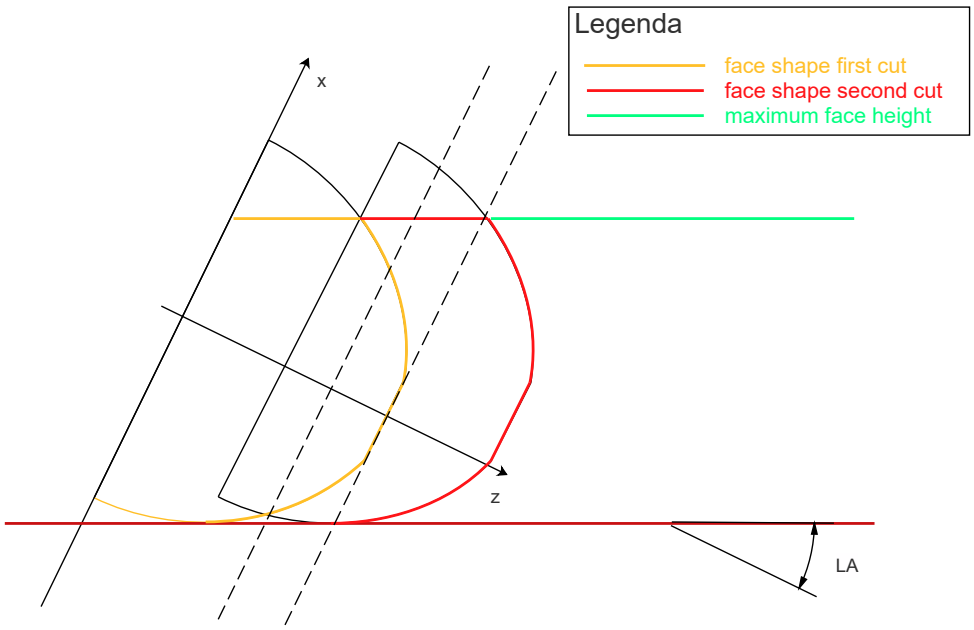

Figure 3.9: The shape of the face cut in rock

[3]Breaching is the occurrence of continued and/or local instabilities on a sandy slope causing a density flow running downwards from the slope (Vlasblom, 2013)

3.4.4 Cutting angle of a tooth tip

Three angles are required to describe the approach angle of a tooth in rock: cutting angle α, wedge angle ζ and clearance angle γ. These three angles are measured with respect to the tangent (see figure 3.10) to the orthocycloid trajectory of a tooth and possess the following relationship:

$$\alpha = \zeta + \gamma \tag{3.18}$$

When a pure circumferential motion of the cutter head is observed, the tangent to the trajectory of a tooth equals the tangent to a circle. But during dredging, the circumferential motion is combined with a translational swing motion. The tangent to the trajectory is now varying. Angles α and γ are changing, β is constant. An angle ζ is present (see figure 3.10). This angle ζ must be subtracted from the maximum angles α_0 and γ_0. The angle ζ equals zero when the swing velocity and circumferential velocity make an angle of 0 or 180 degrees relative to each other. α and γ are reaching a maximum value in that case, which equals α_0 and γ_0. The corrected angles α and γ are written as follows:

$$\alpha = \alpha_0 - \zeta \tag{3.19}$$

$$\gamma = \gamma_0 - \zeta \tag{3.20}$$

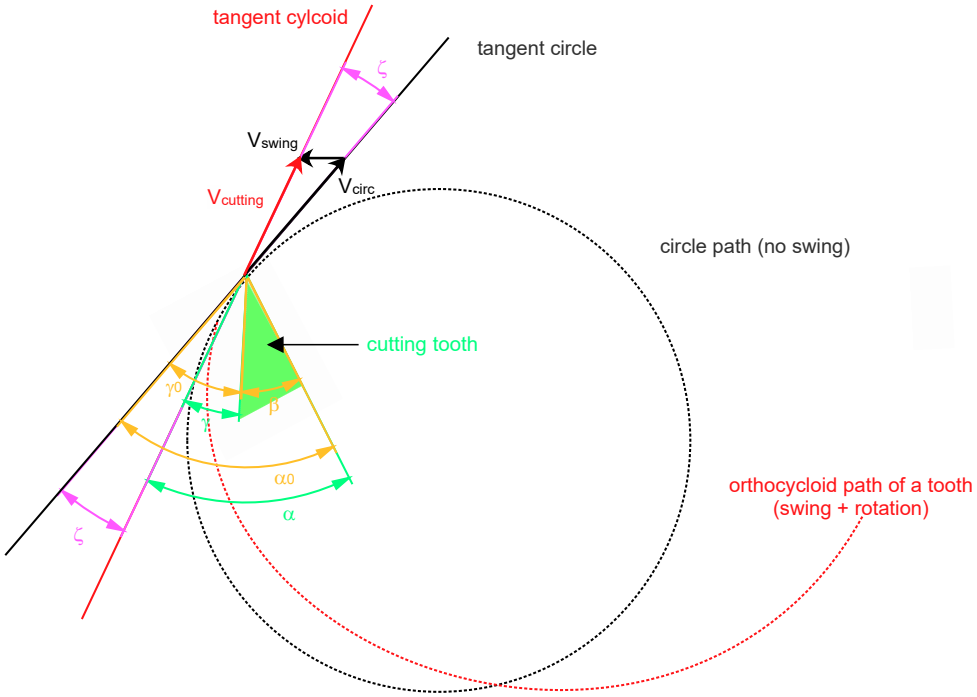

Figure 3.10: Three cutting angles (α, β, γ) corrected for the orthocycloid trajectory of a cutting tooth

Using the cosinus rule, the angle ζ can be calculated.

$$v_{swing}^2 = v_{cut}^2 + v_{circ}^2 - 2 \cdot v_{circ} \cdot v_{cut} \cdot \cos\zeta \tag{3.21}$$

$$\cos\zeta = \frac{v_{swing}^2 - v_{circ}^2 - v_{cut}^2}{-2 \cdot v_{circ} \cdot v_{cut}} \tag{3.22}$$

$$v_{circ} = \omega_{circ} \cdot R \tag{3.23}$$

$$v_{cut}^2 = v_{swing}^2 + 2 \cdot v_{swing} \cdot R \cdot \omega_{circ} \cdot \cos(\theta_{sweep} + \omega_{circ} \cdot t) + R^2 \cdot \omega_{circ}^2 \tag{3.24}$$

Substituting equation 3.23 in equation 3.21 gives:

$$\zeta = \left|\arccos\left(\frac{R \cdot \omega_{circ} + v_{swing} \cdot \cos(\theta_{sweep} + \omega_{circ} \cdot t)}{\sqrt{v_{swing}^2 + 2 \cdot v_{swing} \cdot R \cdot \omega_{circ} \cdot \cos(\theta_{sweep} + \omega_{circ} \cdot t) + R^2 \cdot \omega_{circ}^2}}\right)\right| \tag{3.25}$$

Defining a new parameter λ (equation 3.26) to further simplify equation 3.25 gives:

$$\lambda = \frac{v_{circ}}{V_{swing}} \tag{3.26}$$

$$\zeta = \left|\arccos\left(\frac{\lambda + \cos(\theta_{sweep} + \omega_{circ} \cdot t)}{\sqrt{1 + 2 \cdot \lambda \cdot \cos(\theta_{sweep} + \omega_{circ} \cdot t) + \lambda^2}}\right)\right| \tag{3.27}$$

The angle ζ reaches a maximum when a tooth tip is in the pole position. In figure 3.8, the importance of the pole in the orthocycloid is shown. The pole represents the point where the cutting velocity's horizontal direction is changing. In the pole itself, the cutting velocity is vertical. The velocity triangle is now a right-angled triangle because the angle ϕ (in figure 3.8) measures 90 degrees.

3.4.5 Cutting length

The cutting phase defines if a tooth is within the theoretical bank or not. While the tooth is within the face shape, the theoretical cutting length is calculated. Assuming that all parameters are known (radius, swing velocity, circumferential velocity, face height, p), the cutting length can be calculated using the formula defined by Grincuk and Matyashin (de Boer (1977)):

$$l = 2 \cdot R \cdot \frac{1+\lambda}{\lambda} \cdot \int_0^{\frac{\alpha_1}{2}} \sqrt{1 - k^2 \cdot \sin^2 \omega}\, d\omega + \int_0^{\frac{\alpha_2}{2}} \sqrt{1 - k^2 \cdot \sin^2 \omega}\, d\omega \tag{3.28}$$

where:

$$k = \frac{2 \cdot \sqrt{\lambda}}{1+\lambda} \tag{3.29}$$

$$\omega = \frac{\alpha_{(1)(2)}}{2} \tag{3.30}$$

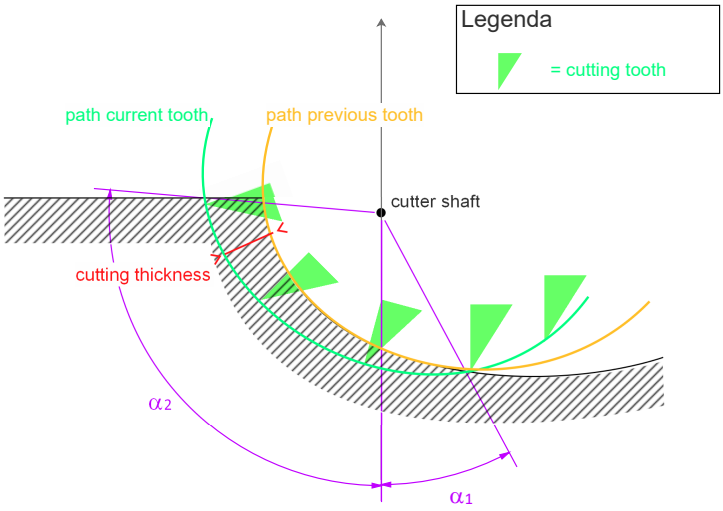

Figure 3.11: Visualizing angles α_1 and α_2

The two angles α_1 and α_2 describe the start and end point of the cutting phase on the tooth path. These angles are visualized in figure 3.11. During the modeling in this research, the theoretical cutting length is calculated to validate the model. The practical cutting length is compared with this theoretical cutting length to indicate the effect of the irregular cutting process on the cutting length of a tooth in contrast to a continuous cutting process (f.e. in clay).

3.4.6 Cutting thickness

Dependent on the amount of teeth within the same plane perpendicular to the cutter axis (plane shown in figure 3.11), the tooth trajectories leave a zone of rock material between each other. This blank space is called the slice that will be excavated when the cutter head is in contact with rock. The shortest distance of a tooth position to the tooth trajectory of the previous tooth within the same contour plane, is called the cutting thickness. The path is dependent on the parameter λ (see equation 3.26) and p (see equation 3.7). The maximum cutting thickness is calculated using the formula:

$$\mathrm{d_{max}} = \frac{1}{\mathrm{p} \cdot \lambda} \tag{3.31}$$

This is the distance traveled during one rotation, divided by the number of teeth located at one height contour line of the cutter head. This maximum cutting thickness is reached at a circumferential angle (θ_t) of -90 degrees during undercutting and 90 degrees during overcutting. Calculating the actual cutting thickness during all other circumferential angles is challenging due to the orthocycloid path of the tooth. The cutting thickness is the perpendicular distance from the tooth trajectory till the free surface of the rock (the trajectory of the previous tooth). To define this thickness, an approximation is given in equation 3.32.

$$\mathrm{d} = |\mathrm{d_{max}} \cdot \sin(\theta_\mathrm{t})| \tag{3.32}$$

The sinus interpolates cutting thickness between 0 (0°) and d_{max} (+/- 90°) and gives a good approximation of the local cutting thickness for each cutting tooth (see figure 3.12). There is no volume difference during under- or overcutting. On the other hand, the shape can differ a lot dependent on λ, p and the swing direction. The cutting length during undercutting is higher compared to overcutting, assuming the same volume is dredged. The direction vector of the cutting depth is required in the further course of this research. Therefore, it is calculated as the cross product of the leading edge direction and the cutting velocity direction (see equation 3.33).

$$\vec{cd} = \vec{le} \times \vec{v}_{\mathrm{cut}} \tag{3.33}$$

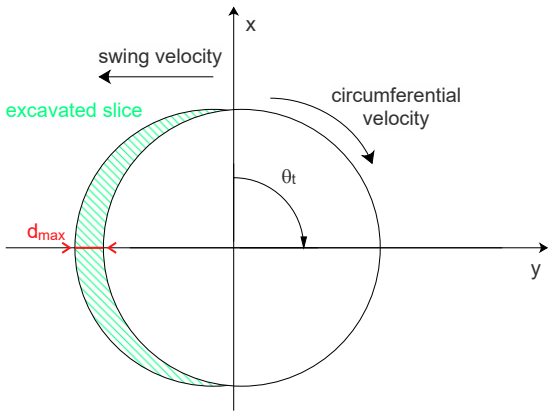

Figure 3.12: Theoretical excavated slice shape and maximum cutting thickness

Chapter 4

Rock fracture mechanics

Rock fracture mechanics is the key to a good modeling of the forces generated during the cutting of rock using a cutter suction dredger. Although very limited rock parameters are available prior to many dredging projects, a good rock model is indispensable. Due to this limited knowledge in advance of a project, the available rock properties must be interpreted as good as possible to create a reliable rock model.

This chapter will start with an introduction to rock properties. The next part of this chapter describes the fracturing of intact and weathered rock. The general failure mechanism is described, followed by the application of the cutting models. The last part of this chapter will explain the theoretical approximation of the chip formation during the fracturing of rock.

4.1 Rock classification

Based on their origin, rocks can be classified in three different categories: igneous, sedimentary and metamorphic rock. Igneous rock originates form the cooling and solidification of magma. It may form with or without crystallization, above or below the earth surface. The magma is formed in the earths mantle or crust and for example deposited by a volcano eruption. Typical examples of igneous rock are basalt and granite. Sedimentary rock is formed through deposition of materials in water, ice or air at the earth surface on dry land or with water on top of it. Typical examples of sedimentary rock are sandstone, limestone and claystone. Metamorphic rock originates from existing rock types by a process called metamorphism. This process recrystallizes the existing rock under specific temperature (greater than 150 degrees Celsius) and pressure (1500 bars) conditions. An example of metamorphic rock is quartzite (Whittaker et al. (1992)).

4.2 Atmospheric rock properties

The cutting of rock with a cutter suction dredger takes place at limited water depths (smaller than 35 meters). The cutting is therefore approximated as atmospheric cutting, whereby the influence of pore pressures is not taken into account. Atmospheric rock can be defined using the following parameters:

UCS = Unconfined Compressive Strength [MPa]

BTS = Brazilian Tensile Strength [MPa]

GSI = Geological Strength Index [-]

ϕ = internal friction angle [°]

δ = external friction angle [°]

Unconfined Compressive Strength

The Unconfined Compressive Strength (UCS) describes the compressive strength of a rock sample. In dredging projects, it is often the only parameter known in advance of a project. A cylindrical part of rock is loaded unconfined axially under compression until failure. The UCS is calculated using equation 4.1 by dividing the force required to fail the rock by the cross sectional area of the core sample (MarCom Working Group 144 (2014)). The Mohr circle[1] of the failure condition is shown in figure 4.1. Point a is the stress state at the failure plane.

$$\sigma_{\text{UCS}} = \frac{\text{F}}{\text{A}} \tag{4.1}$$

where:

σ_{UCS} = Unconfined Compressive Strength [MPa]

F = maximum failure load [N]

A = cross sectional area of core sample [mm^2]

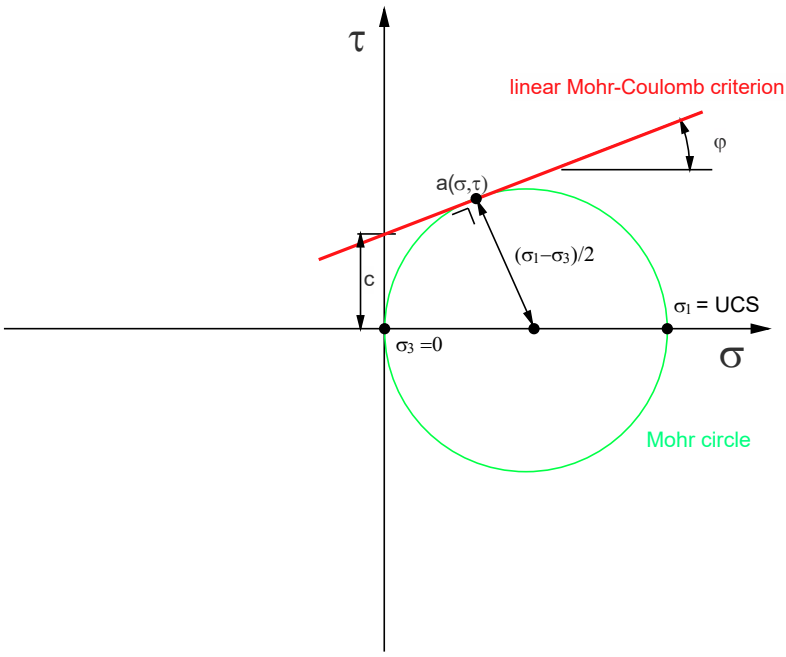

Figure 4.1: Unconfined compressive strenght Mohr circle

Brazilian Tensile Strength

The Brazilian Tensile Strength (BTS) defines the tensile strength of a rock sample. The BTS is also known as the indirect tensile strength. This is due to the fact that this tensile strength is not measured through tensile loading. A cylindrical core sample is loaded unconfined and radial under compression until failure, whereby pure tensile failure occurs. The BTS is calculated using equation 4.2. The Mohr circle of the failure condition is shown in figure 4.2. The sample is loaded by a compressive strength of three times the BTS.

[1]The Mohr circle is a geometric representation of the 2-D transformation of stresses (Lagace (2008))

$$\sigma_{\mathrm{BTS}} = \frac{2 \cdot \mathrm{F}}{\pi \cdot \mathrm{L} \cdot \mathrm{D}} \tag{4.2}$$

where:

σ_{BTS} = Brazilian Tensile Strength [MPa]

F = maximum failure load [N]

L = length of core sample [mm]

D = diameter of core sample [mm]

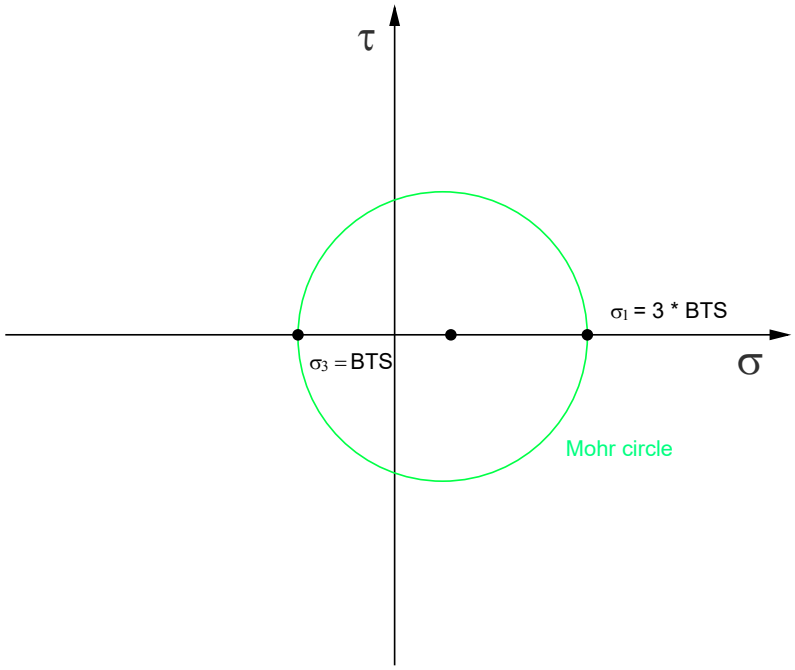

Figure 4.2: Brazilian tensile strength Mohr circle

Geological Strength Index

The Geological Strength Index (GSI) is a measure to classify different types of rock based on interlocking and surface quality of the rock mass (Marinos et al. (2005)). It provides a system to estimate the reduction in rock mass strength for different fracturing conditions. It is useful to choose a GSI-range where a rock mass is classified in. A GSI-range enables a rock mass to be considered as a mechanical continuum without losing the influence geology has on its mechanical properties. The GSI-system is a qualitative measurement tool for rock masses and largely depend on the visual interpretation of the rock mass by an engineer. The general GSI-index chart is shown in figure 4.3.

Cohesion, adhesion, internal and external friction

Internal and external friction are a result of the normal stress and are described by the internal (ϕ) and external friction angle (δ). Internal friction describes the normal stress between the rock grains mutually. External friction describes the normal stress between the rock grains and the grains from another material, like the steel of a cutting tooth. On the contrary, cohesion and adhesion define the attraction force of particles to stick to each other. Cohesion describes the mutual attraction of particles from the same substance. Adhesion describes the sticky effect of molecules from different origins. Cohesion and adhesion are shear stress parameters, independent from normal stress (Miedema (2015)).

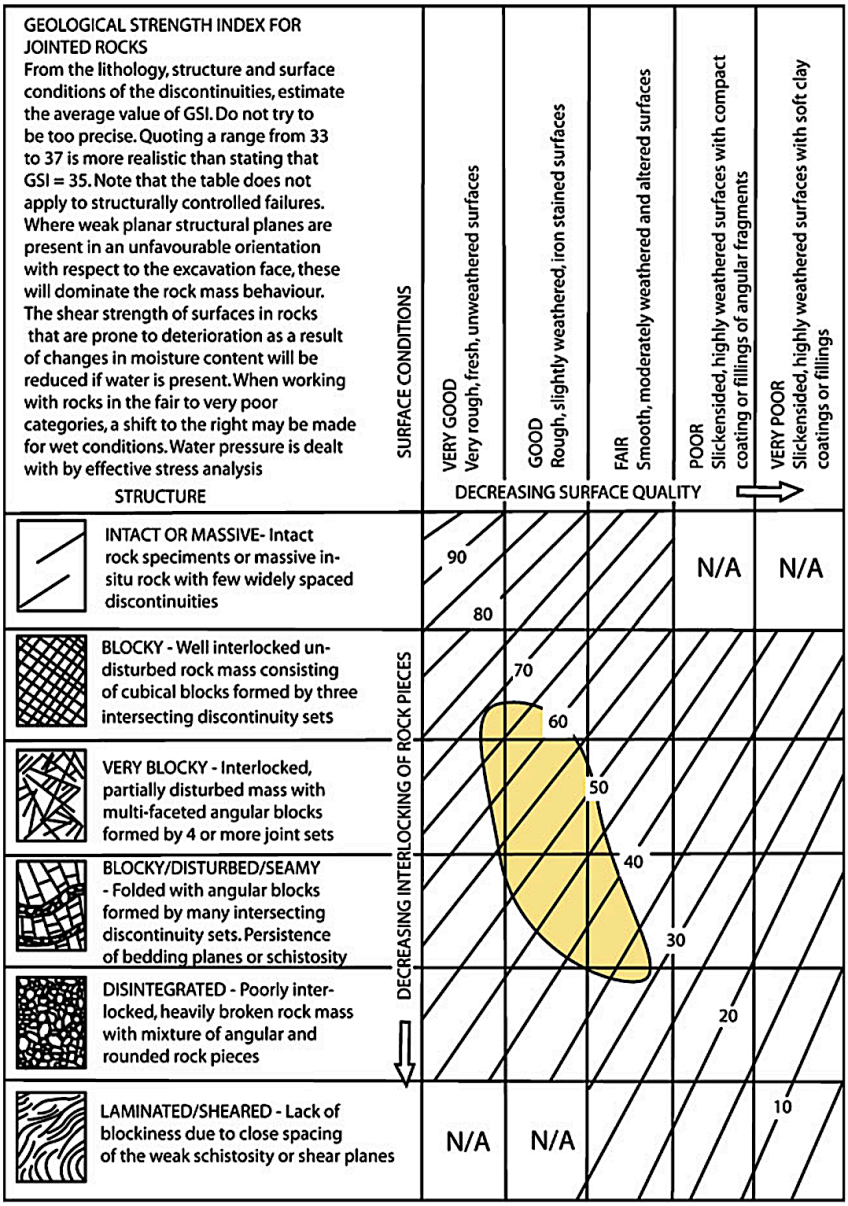

Figure 4.3: General GSI-index chart by Hoek and Brown (Marinos et al. (2005))

4.3 Fracturing of intact rock

The fracturing of rock can occur in two ways: brittle or ductile failure (Miedema (2015)). It is generally accepted that most types of rock will fail brittle during the cutting by a cutter suction dredger due to the high impact velocity and atmospheric conditions. Ductile cutting requires very low cutting velocities and high temperatures or pressures to change the rock characteristics, which is not considered in this research. Only brittle failure will be further investigated.

4.4 Interpretation of rock properties

In the past, many theories are developed describing the cutting process of a tooth in rock. These theories assume a homogeneous rock material. In this research, the effect of irregularities is added using the GSI-index to create a representative reproduction of the reality. A closer look into rock mechanics leads to a better understanding of the problem (Verhoef (1997)).

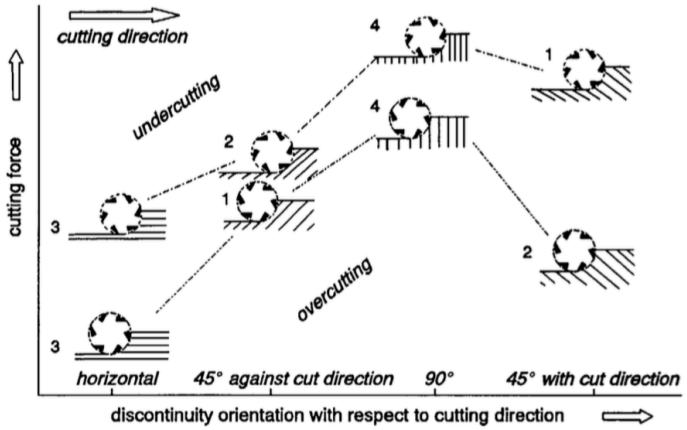

Figure 4.4: The orientation and spacing of discontinuities in function of the cutting force required for excavation (Verhoef (1997))

4.4.1 Discontinuities

A discontinuity refers to the occurrence of joints, cracks, pore spaces and other natural weaknesses within the rock. These discontinuities determine the transmission of stress throughout the rock. The tensile strength in this locality is lower than in the surrounding rock. That is the reason why cracks occur and propagate through these discontinuities. Rock contains discontinuities on small and large scales, where these discontinuities can originate from different natural phenomena (thermal, mechanical or chemical) during the past.

Discontinuities can be divided into four main categories: layering or bedding, joints, shear zones and faults. These categories are based on the geological origin. Discontinuities can be subdivided in singular or systematic discontinuities. They can be part of a network of discontinuities (systematic) which have a common orientation or can be present solely with unique characteristics.

Discontinuity spacing

The spacing between discontinuities is of great importance for the outbreak patterns and forces required to cut rock. When the space between the discontinuities is larger than the cutter head size, the influence of the discontinuities will not be remarkable. In this case, the cutter head will excavate the rock by cutting. On the contrary, when the interspace between discontinuities is smaller than the cutter head, the excavation process will be influenced by the discontinuities. If the penetration depth of a cutting tooth on the cutter head can reach the interspace between the discontinuities, a maximum benefit on cutting force and outbreak pattern can be reached.

Discontinuity orientation

Systematic discontinuities often have a common orientation. This orientation can influence the excavation performance largely. Experiments have shown that an orientation parallel to the haul velocity will have the most favorable influence on the excavation performance. Perpendicular discontinuity orientation requires the highest cutting force.

4.4.2 Rock material and rock mass

In rock excavation a clear distinction must be made between rock material (Dutch: gesteente) and rock mass (Dutch: rots) (Verhoef (1997)). Rock material is the intact and coherent rock. A laboratory test sample is often defined as rock material, but even this small piece of rock (diameter = 55 mm, length = 110 mm) can be extremely fragmented. A distinction can again be made between intact and broken rock material. Rock mass is a larger volume of rock, which will contain fractures over its volume. The division

between rock mass and material became important after the determination that a small rock sample cannot be representative for a rock mass. Rock material defines the microstructure of rock compared to rock mass which describes the structural characteristics of rock. The fundamental different approach of describing rock masses and materials led to different classification systems for both categories. On a small scale, a small piece of rock material can be defined as homogeneous. On a large scale, a batch of rock mass cannot be regarded as homogeneous due to the cracks present. However, rock mass and rock material are interdependent. For dredging purposes, the rock excavation problem is approached as described in the next paragraphs.

The frequency of discontinuities will determine the strength of the rock. An increase in frequency will create a rock mass with a lower strength. When several discontinuities are present the intersections of several fracture planes will define a volume of rock. If these volumes are large compared to the material used for cutting (f.e. a cutter head), the influence of discontinuities is negligible. In case the volumes of rock are rather small compared to the material used for cutting (f.e. smaller than half of the cutter head diameter), the strength of the rock material will reduce significantly. Cutter suction dredgers are mostly cutting rock mass instead of rock material.

The distinction between rock material and rock mass affects the definition of rock excavation. It tends to split the excavation process of rock in three categories: ripping, cutting or a combination of both. Excavating rock by means of loosening and transporting the natural formed rock blocks bounded by discontinuities is called ripping. Cutting is the breakage of rock mass into smaller parts by penetrating the rock until a fracture is generated and a rock block is loosening and can be transported. Most obvious is the appearance of a combination of both. In this case, the fracture frequency as well as the properties of the intact rock are of great importance for modeling the rock behavior during excavation (Verhoef (1997)).

4.5 Fracturing of weathered rock

To incorporate for the discontinuities in the rock mass and rock material, the GSI-value will be estimated to evaluate the excavating process. Hoek and Brown developed a failure criterion to incorporate this GSI-value in the calculation of the internal friction angle and cohesion (Hoek (2006)). A corrected tensile and compressive strength of rock is obtained using this method.

A failure criterion describes which conditions have to be met to initiate the failure of a material. Many failure criteria for rock have been developed in the past. These criteria determine under which combination of normal and shear stress rock will fail. Each failure criterion has its advantages and disadvantages. In dredging science, the Hoek and Brown-failure criterion is widely accepted as one of the most reliable, because this criterion is based on empirical results and incorporates the GSI-value of rock. The criterion is based on the results of research into brittle failure of intact rock by Hoek combined with the results of model studies of fragmented rock mass by Brown. As a starting point, the criterion is based on the properties of intact rock. These properties are reduced dependent on the fragmentation of the rock mass. The GSI-index was chosen to link the empirical criterion to the geological observations.

By applying the Hoek and Brown-failure criterion, it is assumed in this research that the effect of discontinuities is taken into account. A GSI-value of 100 disables the influence. The Hoek and Brown-failure criterion results in a corrected compressive and tensile strength value, cohesion and internal friction angle based on the GSI-value. A GSI-value between 30-70 is common during the modeling of rock, because empirically this is the average GSI-value encountered in rock mechanics (see figure 4.3, yellow zone).

Two types of input parameters can be used to insert the rock parameters in the model. The UCS-, BTS- and GSI-values for a certain rock material can be entered as input parameters or a set of triaxial test data can be entered. For the last option, a corresponding UCS and BTS value is calculated. The corrected compressive and tensile strength of the rock mass are calculated based on the GSI-value.

4.6 Cutting process of rock

A cutting tooth pushed against rock tends to penetrate the rock if the pushing force is high enough. What actually happens is the crushing of rock material around the tooth tip, creating a crushed zone. This crushed zone is formed by cataclastic ductile failure (pseudo-ductile) of the rock, meaning that the microstructure (the 'grain matrix') is destroyed. In rock, this means that the deformation is irreversible. Up to 90 percent of the total cutting energy is spent forming this crushed zone. In this phase of the chip formation process, the failure of rock is defined in the most right part of the failure curve (see figure 4.5, zone IV). This figures represents a PQ-diagram of the stress development around the tooth tip. The definition of P and Q is given in equation 4.3.

$$\begin{aligned} \mathrm{Q} &= \frac{\sigma_1 - \sigma_3}{2} \\ \mathrm{P} &= \frac{\sigma_1 + \sigma_3}{2} \end{aligned} \tag{4.3}$$

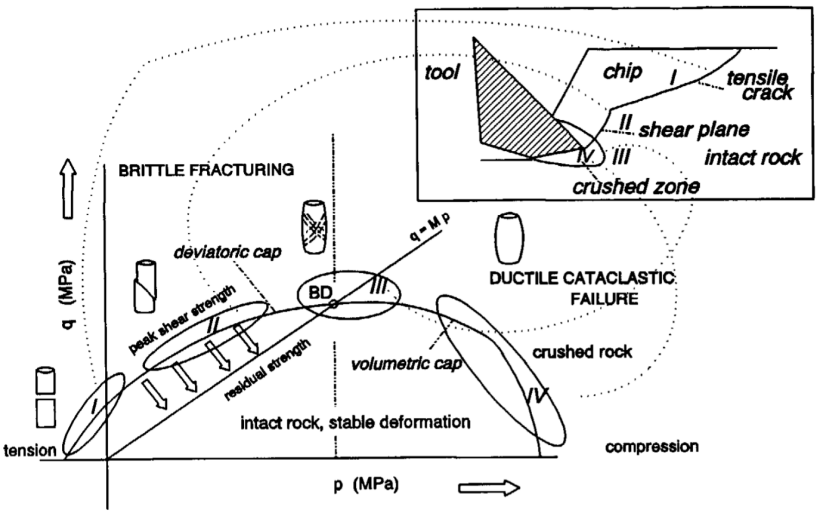

Figure 4.5: The different stages during the formation of a rock chip, Verhoef (1997)

With a small cutting depth, the crushed material around the tooth tip can easily escape towards the surface. With a large cutting depth, this material is locked and will be compacted the more the tooth tip is penetrating the rock. This leads to an increase in stress in the crushed zone (see figure 4.5, zone III). Following the theory that rock will fail and starts to crush at the weakest zones, crushing starts at a very small scale. Large crushed particles will form in front of the tooth tip. The increasing normal stress will crush these particles into smaller particles. This phenomenon will continue till the smallest grains are formed. Fairhurst (1987) described this phenomenon. Extreme high confining stress in front of the tooth tip is present due to friction between the tooth and rock. Forces are transmitted from the crushed zone towards the intact rock through particle to particle contact. The total cutting force applied on the tooth is transmitted through point loads on the intact rock. This point loads may lead to microcrack initiation. This stage in the chip formation is visualized in figure 4.5 at the highest point of the failure curve (Verhoef (1997)).

Next stage in the chip formation is largely dependent on the rock properties. Shear, tensile or a combination of both failure modes may occur. Which one will be present, depends on cutting theories used. Some theories are only valid for a tensile failure mechanism, other can distinguish both types and an intermediate state. In the next paragraphs, these failure types are first discussed in a two-dimensional space. Later, the third dimension is added.

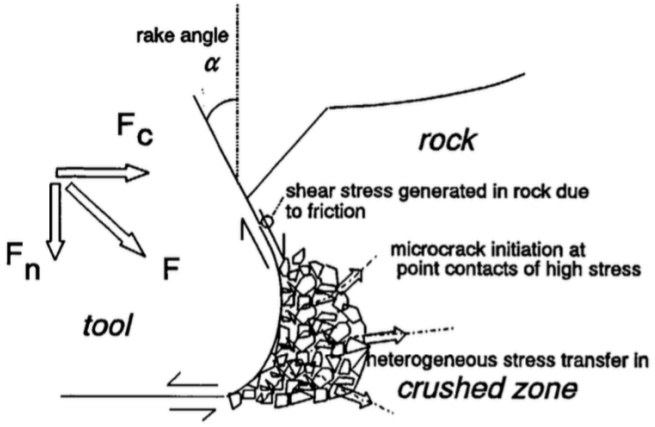

Figure 4.6: Crushing in front of a tooth tip, Verhoef (1997)

Shear failure occurs in relative soft rock types. Soft in terms of rock strength implies that there is a relative small difference between the BTS- and the UCS-value, creating a small Mohr circle and thus a low maximum shear stress value. The rock mass will fail due to its low shear strength. This type of failure is visualized in figure 4.5 as phase II. A shear plane is formed. This plane makes a relative small angle with the vertical. A small piece of rock will break out. The stage of tensile failure is never reached, due to the fact that the shear failure plain will reach the surface of the rock before the maximum tensile stress is reached. The failure plane is almost a straight line under an angle with the vertical.

Tensile failure occurs in brittle rock types. The relative big difference between BTS and UCS will create a Mohr circle with a higher radius than during shear failure. This higher radius means a higher maximum shear stress value. The rock mass will fail due to its low tensile strength. In case of pure brittle failure, stage II in figure 4.5 is skipped and a tensile failure plane is formed (stage I in figure 4.5). This tensile failure plane makes a much bigger angle with the vertical compared with the shear failure plane. A much bigger chip is excavated.

The transition from brittle tensile to brittle shear failure is marked by a transition zone. In between both failure mechanisms, a combination of shear and tensile failure occurs. The chip formation will now exists out of all phases (I till IV) shown in figure 4.5. After microcracks are formed, a shear plane will form and shear failure will occur. During the formation of this shear plane, the maximum tensile stress is reached and a tensile failure plane will originate from the end of the shear failure plane. As shown in figure 4.5, this plane makes an angle with the vertical which is an interpolation between the tensile and shear failure plane.

In this model, the crushing is not incorporated due to the very small penetration depths of the crushing phenomenon (< 1 mm). The accuracy of the model, which is explained later in this chapter is not high enough to model this effect.

4.7 Modeling rock

4.7.1 Building a discrete rock model

A rock mass is modeled by a matrix of structures. Each matrix cell represents a rock part of one cubic centimeter. The dimensions of a rock cube determine the accuracy of the model. One centimeter accuracy is chosen to be an optimal dimension, considering computing time and realistic modeling. A rock cube is shown in figure 4.7, giving its dimensions and orientation in the rock matrix coordinate system.

The rock matrix consists out of a variable number of rock cubes. The rock matrix is built beforehand, based on following parameters:

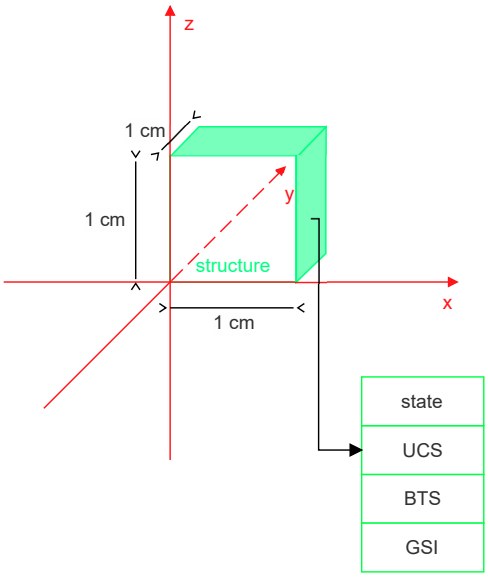

Figure 4.7: Definition of a rock cube

- pontoon parameters
  - maximum swing angle
  - swing velocity
  - swing radius
- cutter head parameters
  - rotational velocity
  - cutter head dimensions
- number of rotations

To limit the size of the rock matrix, a matrix is built custom fit around the cutter head working area based on the previous mentioned parameters. At the bottom and sides of the cutter head working area, an extra 50 centimeters is built, to incorporate the break out of parts in the rock mass outside the cutter head outer dimensions. Each rock cube position is defined by three-dimensional coordinates. A sample part from a rock matrix is shown in figure 4.8. The rock mass dimensions and shape, automatically calculated by the cutter head dimensions and path, can at all times be overruled by user defined values.

To create a rock matrix with varying properties, each rock cube must contain a list of cell specific parameters. A rock cube is therefore programmed as a structure with different sub-variables. The list of sub-variables is extensible, but initially contains the UCS-, BTS- and GSI-value. To detect rock cubes, the state is also stored as a sub-variable which defines if a rock cube is already cut or not. Figure 4.7 shows the rock cube with its structure and sub-variables.

The rock matrix can be programmed to have different vertical, horizontal or inclined layers of rock strength parameters, which is often the case in rock models created by geologists. In many cases, the rock matrix will become too big for the RAM-memory of the computer used for the simulation. This problem is solved by creating a .mat-file which contains the complete matrix. By using the *matfile* function in Matlab, only the required part of the matrix is loaded into the memory for reading and writing purposes.

4.7.2 The rock matrix coordinate system

To model the cutter head within the rock matrix, the coordinates must be transformed to this matrix coordinate system. This reference frame is set up with its origin in the non-existing cell (0,0,0) of the

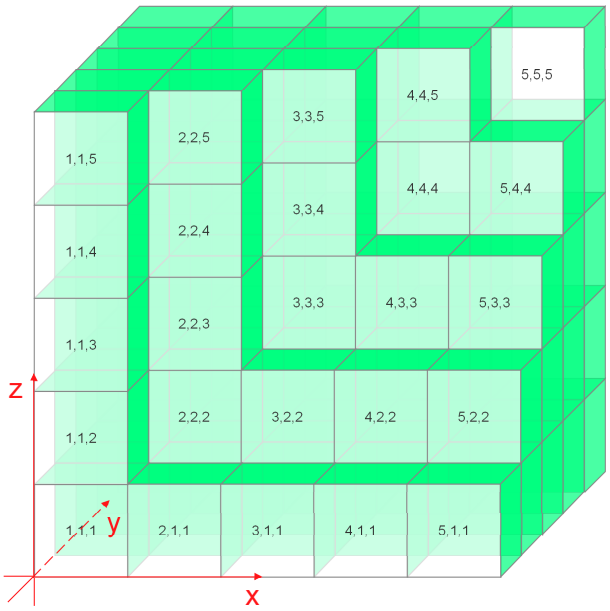

Figure 4.8: Definition of the rock matrix

rock matrix. The cell indices indicate the position of a rock cube and can be linked to the cutter head tooth coordinates. This method is used to link the location of the rock cubes to the cutter head positions. The reference frame was already mentioned in chapter 3, section 3.3. The cutting tooth positions are transformed from the tooth coordinate system to the rock matrix coordinate system (coordinate system 0).

It must be noted that all cells with an index equaling 0 do not exist. The lower boundaries of the rock matrix are defined as the cells with indices (1,:,:), (:,1,:) and (:,:,1), while the cell ranges (0,:,:), (:,0,) and (:,:,0) do not exist. Therefore, the cutter head coordinates are added by 1 unit to make it physically correct. If a tooth tip is located in position (0,0,0) in the rock matrix coordinate system, this position is transformed to position (1,1,1). The upper boundaries of the rock matrix are the cells with indices (end,:,:), (:,end,:) and (:,:,end).

4.8 Forces generated during the cutting process

Forces generated during the cutting of rock were until now only modeled in a two-dimensional space. The goal in this research is to model these forces in three dimensions. The current two-dimensional cutting theories will be used as a starting point. The four cutting theories generally accepted as trustworthy are:

1: model of Miedema

2: model of Evans for a pick point

3: model of Merchant

4: model of Nishimatsu

The input required for these models are the rock parameters, tooth frontal area and orientation. All the rock parameters were already discussed in the previous sections of this chapter and are listed on the next page. It is assumed that the external friction angle is approximated by $\frac{2}{3}$ times the internal friction angle. The tensile strength is defined as a negative value, the compressive strength as a positive value.

- ϕ = internal friction angle [°]
- δ = external friction angle ($\frac{2}{3} \cdot \phi$) [°]

- c = cohesion [MPa]
- σ_t = tensile strength [MPa]
- σ_c = compressive strength [MPa]

The tooth parameters required are the cutting angle, the width of the leading edge and cutting depth encountered.

- α = cutting angle [°]
- w = width of the leading edge [m]
- h = cutting depth of the tooth tip [m]

The existing cutting theories describe the forces required to create a crack in a two dimensional space. This crack is initiated in a specific direction: the shear angle β, which is calculated based on the principle of minimum energy. The shear angle is measured from the horizontal. In this research, the model of Miedema is used as a starting point, but the other cutting models are also validated. The cutting model of Miedema is discussed in the next section.

4.8.1 Miedema

The cutting model of Miedema defines the forces implied during brittle-shear failure, brittle-tensile failure and the transition between those two. Each of these failure mechanisms is characterized by a type of breakout shape: the shear type (shear failure), tear type (tensile failure) or a combination of both, the chip type (shear/tensile failure). The cutting model defines the shear plane of the breakout shape, but does not describe a method to create a lateral breakout volume. The lateral breakout angle assumption is further discussed in section 4.9.

Although the cutting process is categorized by three different types, the force balance is based on the same principle and is visualized in figure 4.9. A distinction is made between the forces on the layer cut and the forces on the blade. A vertical and horizontal balance is set up to compute the missing cutting force K_2.

According to Miedema (2015), the forces on the layer cut are:

N_1 = normal force acting on shear surface resulting from effective grain stresses

S_1 = shear force resulting from internal friction

C = force resulting from pure cohesion (τ_c)

N_2 = normal force resulting from effective grain stresses

S_2 = shear force resulting from external friction

The forces on the blade become:

N_2 = normal force resulting from effective grain stresses

S_2 = shear force resulting from external friction

The forces N and S can be combined to an equivalent force K, given in formula 4.4.

$$K = \sqrt{N^2 + S^2} \tag{4.4}$$

The horizontal equilibrium of forces becomes:

$$\sum F_h = K_1 \cdot \sin(\beta + \phi) + C \cdot \cos(\beta) - K_2 \cdot \sin(\alpha + \delta) = 0 \tag{4.5}$$

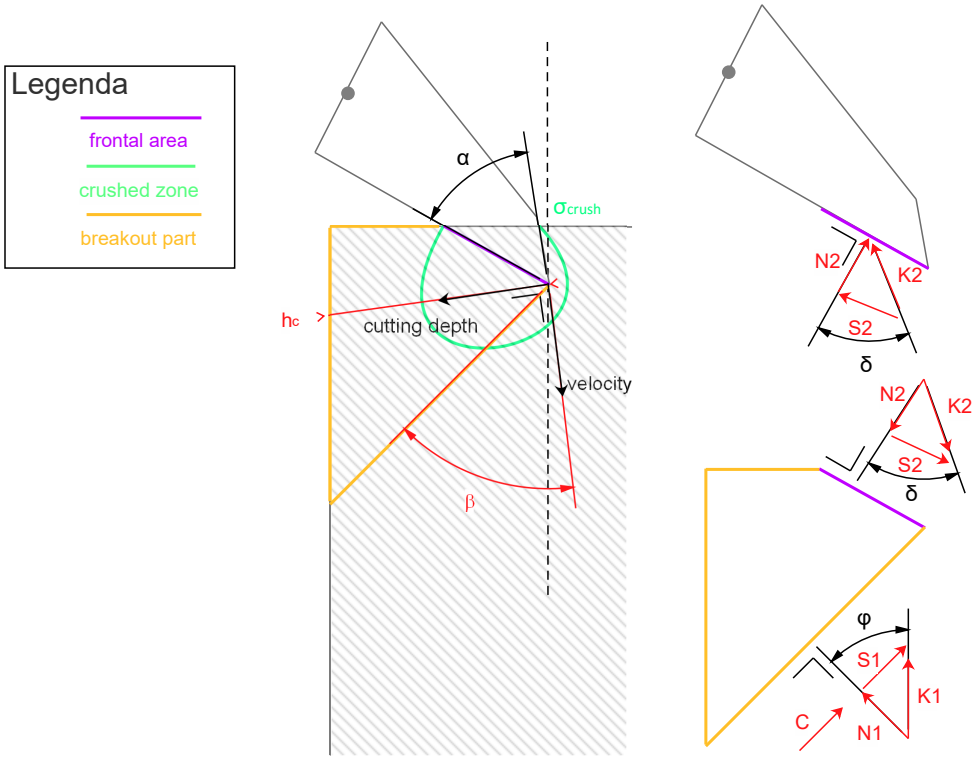

Figure 4.9: Miedema's force balance during cutting process (Miedema (2014))

The vertical equilibrium of forces becomes:

$$\sum \mathrm{F_h} = \mathrm{K_1} \cdot \sin(\beta + \phi) + \mathrm{C} \cdot \cos(\beta) - \mathrm{K_2} \cdot \sin(\alpha + \delta) = 0 \tag{4.6}$$

The force C is the cohesive force acting on the shear plane and equals the cohesive strength multiplied by the area of the theoretical shear plane (equation 4.7).

$$\mathrm{C} = \frac{\mathrm{c} \cdot \mathrm{h_1} \cdot \mathrm{w}}{\sin(\beta)} \tag{4.7}$$

Given the horizontal and vertical force balance (equations 4.5 and 4.6), the two unknown forces $\mathrm{K_1}$ and $\mathrm{K_2}$ can be derived. The force $\mathrm{K_1}$ equals:

$$\mathrm{K_1} = \frac{-\mathrm{C} \cdot \cos(\alpha + \beta + \delta)}{\sin(\alpha + \beta + \delta + \phi)} \tag{4.8}$$

The force $\mathrm{K_2}$ equals:

$$\mathrm{K_1} = \frac{\mathrm{C} \cdot \cos(\phi)}{\sin(\alpha + \beta + \delta + \phi)} \tag{4.9}$$

The total force on the blade ($\mathrm{K_2}$) can be decomposed in a component parallel with the cutting velocity ($\mathrm{F_h}$, equation 4.10) and a component perpendicular to this cutting velocity ($\mathrm{F_v}$, equation 4.11).

$$\mathrm{F_h} = \mathrm{K_2} \cdot \sin(\alpha + \delta) \tag{4.10}$$

$$\mathrm{F_v} = \mathrm{K_2} \cdot \cos(\alpha + \delta) \tag{4.11}$$

Substituting equation 4.9 into equations 4.10 and 4.11 leads to the total horizontal and vertical force component of the Miedema cutting model. These both formulas (equation 4.12 and 4.13) are entered in the model to calculate the cutting forces.

$$F_h = \frac{c \cdot h_i \cdot w \cdot \cos(\phi) \cdot \sin(\alpha + \delta)}{\sin(\beta) \cdot \sin(\alpha + \beta + \delta + \phi)} \tag{4.12}$$

$$F_v = \frac{c \cdot h_i \cdot w \cdot \cos(\phi) \cdot \cos(\alpha + \delta)}{\sin(\beta) \cdot \sin(\alpha + \beta + \delta + \phi)} \tag{4.13}$$

To simplify formulas 4.12 and 4.13, Miedema introduced a factor λ which incorporate all the trigonometric entities for the horizontal (λ_h) and vertical (λ_v) force component. The factor differs for brittle-tensile and brittle-shear failure. For the transition zone between both failure mechanisms, an interpolated value is obtained.

Brittle-shear failure

For brittle-shear failure, the standard formulas derived by Miedema can be applied (equation 4.12 and 4.13). These formulas are decomposed using the coefficient λ in equations 4.14 and 4.15.

$$\begin{aligned} F_{h,s} &= \lambda_{h,s} \cdot c \cdot h_{uncut} \cdot w \\ \lambda_{h,s} &= \frac{\cos\phi \cdot \sin(\alpha + \delta)}{\sin\beta \cdot \sin(\alpha + \beta + \delta + \phi)} \end{aligned} \tag{4.14}$$

$$\begin{aligned} F_{v,s} &= \lambda_{v,s} \cdot c \cdot h_{uncut} \cdot w \\ \lambda_{v,s} &= \frac{\cos\phi \cdot \cos(\alpha + \delta)}{\sin\beta \cdot \sin(\alpha + \beta + \delta + \phi)} \end{aligned} \tag{4.15}$$

The principle of minimum energy is applied to evaluate the angle β. The cutting forces (equations 4.14 and 4.15) reach their minimum when the denominator reaches its maximum. This maximum is obtained using an iterative method, but can also be achieved by taking the derivative of the denominator with respect to β. The general formula for β after derivation becomes:

$$\beta = \frac{\pi}{2} - \frac{\alpha + \delta + \phi}{2} \tag{4.16}$$

Brittle-tensile failure

A new parameter c_m is defined. This parameter represents the mobilized cohesion of rock and is a pseudo-cohesion value which allows to calculate the tensile failure cutting forces by using the cutting formulas for shear failure. The c_m-value is found by solving equation 4.17, which states the condition for tensile failure. In equation 4.18, equation 4.17 is solved for c_m.

$$\frac{\sigma_t}{c_m} < -\frac{\cos(\alpha + \beta + \delta)}{\sin(\alpha + \beta + \delta + \phi)} \cdot (\cos\phi - \tan\phi + \tan\phi \cdot \sin\phi) + \tan\phi - \frac{1}{\cos\phi} \tag{4.17}$$

$$c_m = \sigma_t \cdot \left[\left(\frac{\sin\left(\frac{\alpha+\delta-\phi}{2}\right)}{\cos\left(\frac{\alpha+\delta+\phi}{2}\right)} - 1 \right) \cdot \left(\frac{1 - \sin\phi}{\cos\phi} \right) \right]^{-1} \tag{4.18}$$

The parameter λ is calculated beforehand to preserve the overview of the force formula. The cutting force formulas are given in equations 4.19 and 4.20.

$$\begin{aligned} F_{h,t} &= \lambda_{h,t} \cdot c_m \cdot h_{uncut} \cdot w \\ \lambda_{h,t} &= \frac{\cos\phi \cdot \sin(\alpha + \delta)}{\sin\beta \cdot \sin(\alpha + \beta + \delta + \phi)} \end{aligned} \tag{4.19}$$

$$\begin{aligned} \mathrm{F_{v,t}} =& \lambda_{\mathrm{v,t}} \cdot \mathrm{c_m} \cdot \mathrm{h_{uncut}} \cdot \mathrm{w} \\ \lambda_{\mathrm{v,t}} =& \frac{\cos\phi \cdot \cos(\alpha+\delta)}{\sin\beta \cdot \sin(\alpha+\beta+\delta+\phi)} \end{aligned} \tag{4.20}$$

The shear angle β is evaluated in the same way as during shear failure. The difference is that the derivation of the denominator of the cutting forces is more complex because of the extra terms introduced by the mobilized cohesion. The difference in shear angle between brittle-shear and brittle-tensile failure is 15°.

$$\beta = \frac{\pi}{2} - \frac{\frac{\pi}{6} + \alpha + \delta + \phi}{2} \tag{4.21}$$

Transition between brittle-shear and brittle-tensile failure

During the transition between brittle-shear and brittle-tensile failure, a linear interpolation is used to calculate the cutting forces (Miedema (2015)). For this interpolation, a coefficient f is introduced.

- brittle-tensile rock failure: $f = 1$
- brittle-shear rock failure: $f = 0$
- brittle-shear/tensile rock failure: $0 < f < 1$

Equations 4.22, 4.23 and 4.24 show the interpolation formulas.

$$\mathrm{F_{h,st}} = \mathrm{F_{h,t}} \cdot (1-f) + \mathrm{F_{h,s}} \cdot f \tag{4.22}$$

$$\mathrm{F_{v,st}} = \mathrm{F_{v,t}} \cdot (1-f) + \mathrm{F_{v,s}} \cdot f \tag{4.23}$$

$$\beta_{\mathrm{st}} = \beta_{\mathrm{t}} \cdot (1-f) + \beta_{\mathrm{s}} \cdot f \tag{4.24}$$

The factor f is defined by calculating the upper and lower tensile strength values based on the Mohr circles of shear and tensile failure. The highest tensile strength value (absolute value) defines the lower boundary of shear failure. Above this value, shear failure occurs. The lowest tensile strength value (absolute value) defines the upper boundary of tensile failure. Below this value, tensile failure occurs. In between both values, a transition zone describes the intermediate phase between tensile and shear failure.

Both values are calculated by implementing the condition in equation 4.17 for both the shear angle for brittle-shear and brittle-tensile failure. A ratio is obtained for each of these two shear angles (see equation 4.25). Substituting the cohesion (c, see equation 4.26) and shear angle (β, see equations 4.16 and 4.21) in each of these ratios leads to a ratio UCS/BTS. For a given UCS-value, two σ_t-values can be obtained that define the tensile strength limits of shear and tensile failure.

$$\frac{\sigma_{\mathrm{t}}}{c} < -\frac{\alpha+\beta+\delta}{\alpha+\beta+\delta+\phi} \cdot (\cos(\phi) - \tan(\phi) + \tan(\phi)\cdot\sin(\phi)) + \tan(\phi) - \frac{1}{\cos(\phi)} \tag{4.25}$$

$$\mathrm{c} = \frac{\mathrm{UCS}}{2} \cdot \left(\frac{1-\sin\phi}{\cos\phi}\right) \tag{4.26}$$

$$\sigma_{\mathrm{t_{max,min}}} = \frac{\mathrm{UCS}}{2} \cdot \left(\frac{\sin\left(\frac{\alpha+\delta-\phi}{2}\right)}{\cos\left(\frac{\alpha+\delta+\phi}{2}\right)} - 1\right) \cdot \left(\frac{1-\sin\phi}{\cos\phi}\right)^2 \tag{4.27}$$

Using equation 4.27 the two limiting tensile stress values are obtained by using the two substituted β-values of shear and tensile failure. The tensile strength of the rock mass (BTS) must be compared with these two values. It is to be noticed that absolute tensile strength values are used. If the tensile strength is lower than $\sigma_{\mathrm{t,min}}$, factor f equals 1 and brittle-tensile failure occurs. If the tensile strength is higher than $\sigma_{\mathrm{t,max}}$, factor f equals 0 and brittle-shear failure occurs. In between $\sigma_{\mathrm{t,max}}$ and $\sigma_{\mathrm{t,min}}$, factor f is linear interpolated between 0 and 1 and the failure is an interpolation between brittle-tensile and brittle-shear stress.

- $|\text{BTS}| > |\sigma_{\text{t,max}}|$

  $f = 1$, tensile failure

- $|\text{BTS}| < |\sigma_{\text{t,min}}|$

  $f = 0$, shear failure

- $|\sigma_{\text{t,min}}| < |\text{BTS}| < |\sigma_{\text{t,max}}|$

  $0 < f < 1$, shear/tensile failure

The influence of the cutting angle α

The cutting angle α has a major influence on the type of rock failure. Figure 4.10 indicates the cutting angle which is common during rock cutting (68°) with a magenta line. It can be concluded this cutting angle implies that no tensile failure can occur. Tensile failure can only be caused by reducing the cutting angle. The influence of the cutting angle on the cutting forces is dependent on the rock mass parameters (cohesion and tensile strength). For most rock types, a tensile failure mechanism generates higher peak but lower average loads.

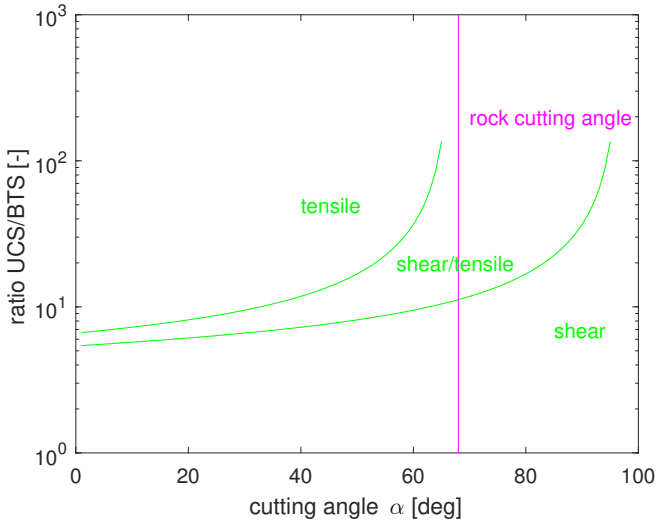

Figure 4.10: Graph indicating which type of failure occurs ($\phi = 35°$)

4.9 Theoretical breakout shapes

Each of the cutting models calculate the direction of the shear plane along which the rock will fail, but a three-dimensional shape is not defined. Therefore, some assumptions are required to define the boundaries of the rock chip excavated corresponding the forces calculated. Three different shapes are defined for each type of rock failure: shear, tensile and shear/tensile failure. The cutting coordinate system is used as a reference frame to define the boundaries of the chip.

The cutting models do not define the lateral breakout angle of the breakout part. This lateral angle is based on empirical results by Alvarez Grima et al. (2015). In this research, a lateral angle of 30° with the vertical is assumed. Dependent on the cutting velocity, the angle varies. This varying lateral breakout angle is visualized in figure 4.11a for low cutting velocities and figure 4.11b for high cutting velocities. For high cutting velocities, the lateral breakout angle is approximately 30 ° with the vertical, for low cutting velocities it is approximately 45 ° with the vertical. During the excavation with typical cutter head, the velocities encountered are approximately between 1 and 2 m/s.

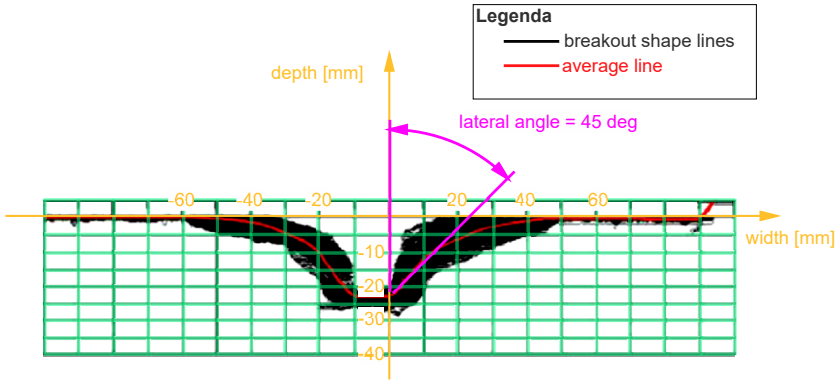

(a) low velocity (0.2 m/s) lateral cut pattern

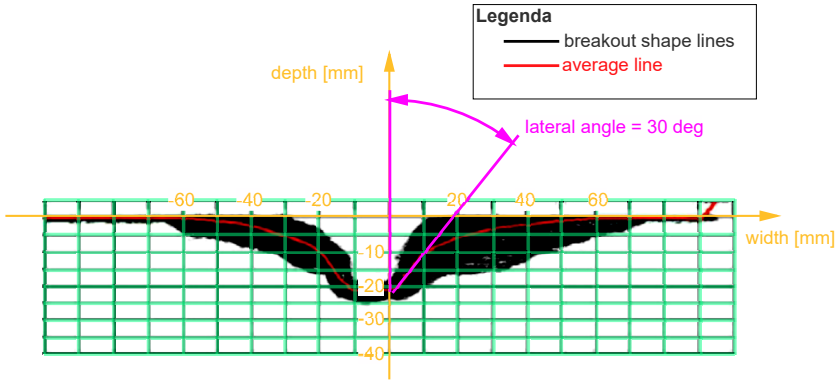

(b) high velocity (2 m/s) lateral cut pattern

Figure 4.11: Lateral breakout angle test results by Alvarez Grima et al. (2015)

4.9.1 Shear failure

The chip boundaries during shear failure are visualized in figure 4.12. Starting from the two end positions of the leading edge (T and T'), a boundary is directed in the positive x-direction towards the rock surface (A and A') under an angle β (shear angle) with the horizontal (see figure 4.12c). In the negative x-direction, the rock surface (B and B') is reached under an angle α (cutting angle) with the horizontal (see figure 4.12c). This line simulates the tooth cutting face. The leading edge is the fixed width of the breakout shape at the lower chip boundary.

A lateral angle θ must be predefined to model the lateral shape of the breakout part (see figure 4.12a). This is the complementary angle of the approximated lateral breakout angle. At every position along the lines TB, T'B', TA and T'A', a lateral boundary is directed towards the rock surface under an angle θ with the horizontal. For this reason, the boundaries in the top view become narrower near the forward end of the shape. At the tooth tip, the lateral boundaries are the lines TC and T'C'.

4.9.2 Shear/tensile failure

The chip boundaries during shear/tensile failure are visualized in figure 4.13. Starting from the two end positions of the leading edge (T and T'), the intersection of the rock surface with the shear plane is calculated (A and A'). The shear plane is drawn in the positive x-direction under an angle β (shear angle) with the horizontal (see figure 4.13c). Between this intersection (A and A') and the leading edge (T and T'), an elliptical line is drawn and forms the forward boundary of the breakout part. In the negative x-direction, the rock surface (B and B') is reached under an angle α (cutting angle) with the horizontal (see figure 4.13c). This line simulates the tooth cutting face. The leading edge is the fixed width of the breakout shape at the lower chip boundary.

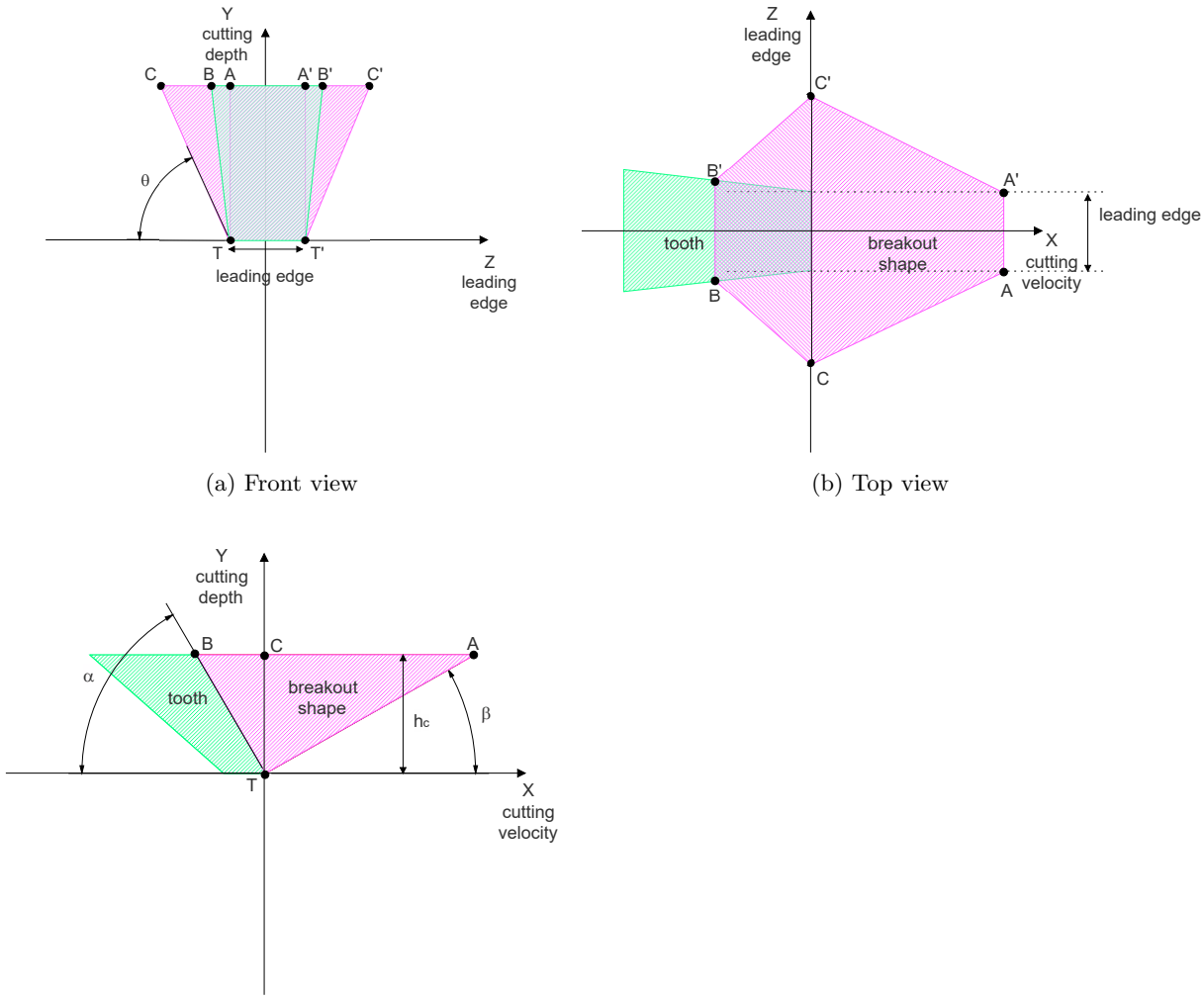

(a) Front view

(b) Top view

(c) Side view

Figure 4.12: Shear failure breakout shape

A lateral angle θ must be predefined to model the lateral shape of the breakout part (see figure 4.13a). This is the complementary angle of the approximated lateral breakout angle. Again, the intersection of the rock surface with the lateral shear plane is calculated (C and C' for the tooth tip). This point C is calculated for every position along the lines TB, T'B', TA and T'A'. Between the lateral intersection with the rock surface and the corresponding forward position along the forward elliptic boundary, an elliptic line is drawn in the YZ-plane and forms the lateral boundary of the breakout part (see figure 4.13a).

4.9.3 Tensile failure

The chip boundaries during tensile failure are visualized in figure 4.14. Starting from the two end positions of the leading edge (T and T'), a boundary is directed in the positive x-direction away from the rock surface under an angle $-(\phi - \beta)$ with the horizontal (see figure 4.14c). For a distance which equals 2 times the cutting depth, a boundary is created (TD and T'D'). From the point D (or D') on, the boundary direction is turned 90 degrees upwards to reach the rock surface in point A (or A'). In the negative x-direction, the rock surface is reached under an angle α (cutting angle) with the horizontal (see figure 4.14c). This line simulates the tooth cutting face. The leading edge is the fixed width of the breakout shape at the lower chip boundary.

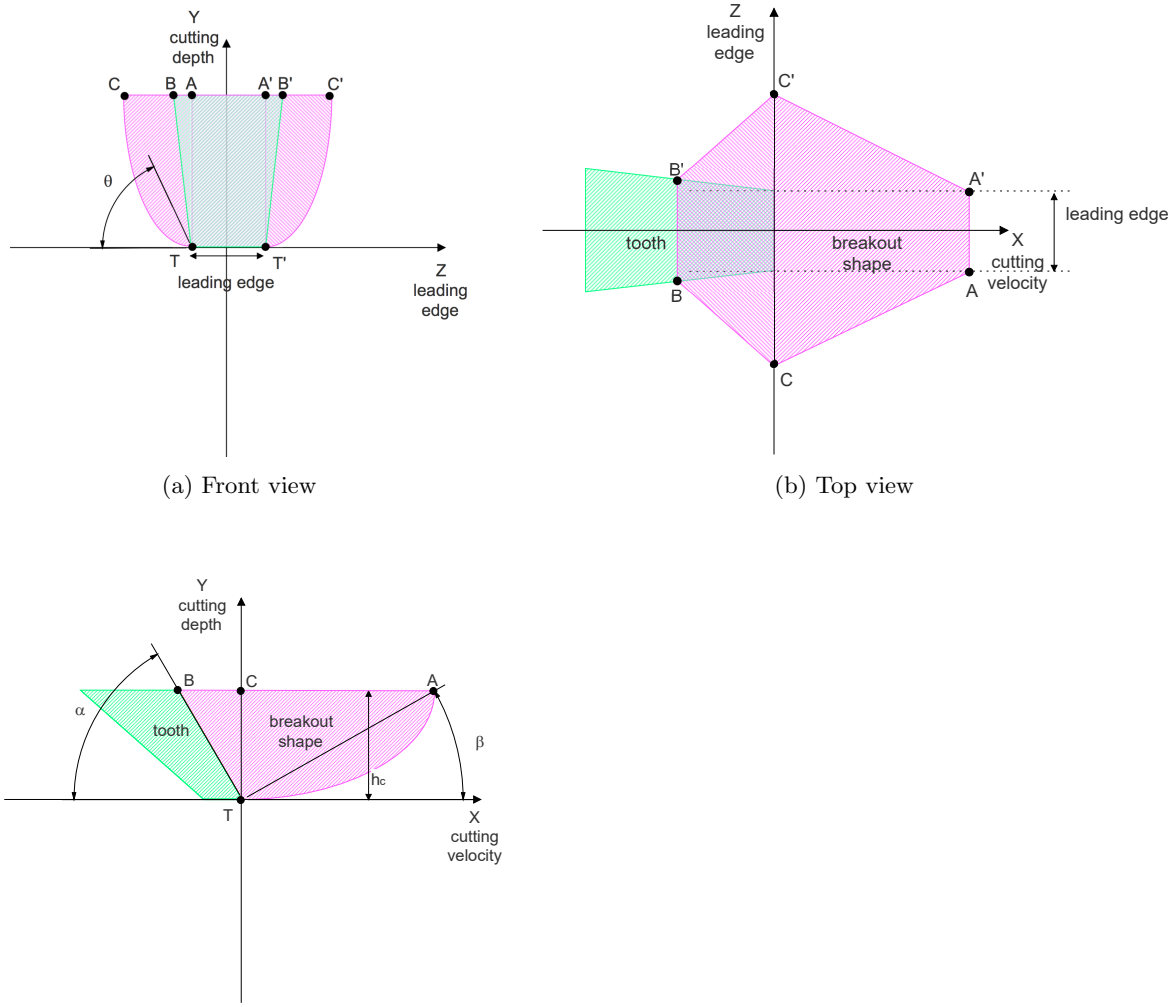

(a) Front view

(b) Top view

(c) Side view

Figure 4.13: Shear/tensile failure breakout shape

A lateral angle θ must be predefined to model the lateral shape of the breakout part (see figure 4.14a). This is the complementary angle of the approximated lateral breakout angle. At every position along the lines TB, T'B', TA and T'A', a boundary is directed towards the rock surface under an angle θ with the horizontal. At the tooth tip, this is the line TC and T'C'.

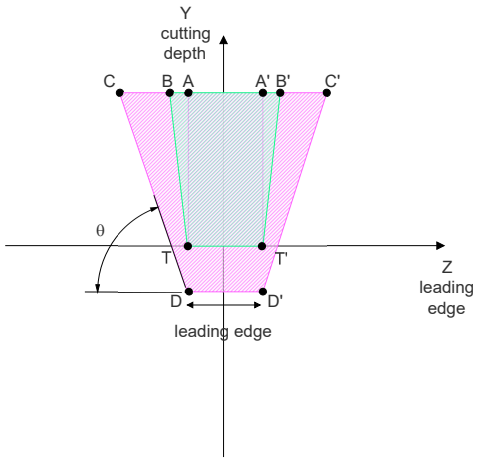

(a) Front view

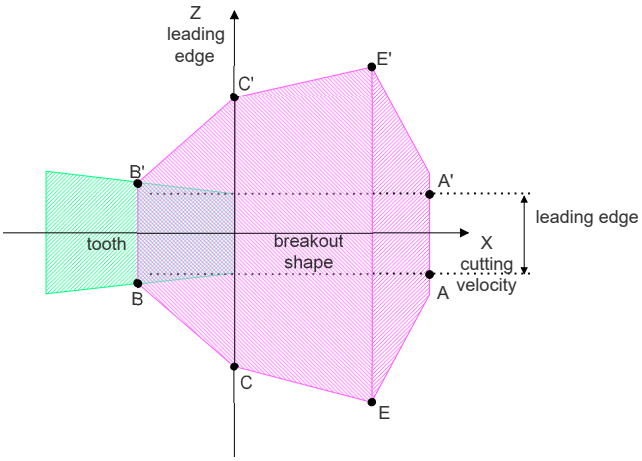

(b) Top view

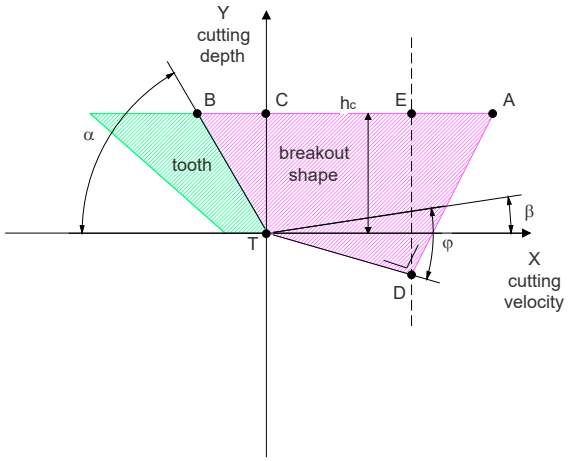

(c) Side view

Figure 4.14: Tensile failure breakout shape

Chapter 5

Conclusions and recommendations

5.1 Resume

A geometric model is built to simulate the motions of a cutter head mounted on a cutter suction dredger. This model incorporates the swing, circumferential and step motion of a cutter head. The path of a tooth tip is modeled in a discrete manner. The orientation of a tooth is simulated as accurate as possible, including the cutting angle correction for the swing velocity.

A rock model is created which takes into account the compressive and tensile strength parameters of the rock material in combination with the weathered state of the rock mass. The weathered state parameters of the rock mass, including the discontinuity properties, are included in the GSI-value. The intact rock material properties are converted to an equivalent value for the weathered rock mass. A method developed by Hoek (2006) based on empirical results is used to calculate the equivalent rock properties.

The software created in this research is a combination of a geometric and a rock model. The interaction of both models is simulated. The typical cutting models (Miedema, Evans, Merchant and Nishimatsu) are used as a starting point for calculating the excavation forces and describing the two-dimensional breakout shapes. These models have been extended to the three-dimensional space by defining a lateral breakout shape based on empirical results by Alvarez Grima et al. (2015).

Many issues were encountered during the adjustment of the model. The definitions of rock chips in the rock matrix based on the position and orientation of teeth was a challenging mission. Small cutting depths were often encountered while a large rock chip was excavated. These unrealistic cutting patterns led to the development of an intrusion criterion, which has ensured a smooth build up of excavation forces. The aim of this intrusion criterion is to model the penetration of a cutting tooth in the rock mass. Without this criterion, the tooth would break out a complete rock chip at every time step a rock cube was detection. Another issue was the tolerance of rock cubes being excavated. A shape is created which is excavated. Due to the fact that often a small shape is defined in combination with the accuracy of the model (1 cm^3), a great distinction in force signal on a cutting tooth was present. All these issues are tackled and solved, leading to a stable model.

The heart of the model is a method to approximate the cutting forces based on the volume or failure surface of the rock chip being excavated. The theoretical cutting models does not seems to assess the cutting forces very well in reality. Small cutting forces were encountered during the excavation of large chips while large cutting forces were encountered during the excavation of small chips. This issue was tackled by the development of a cutting force correction algorithm. This algorithm scales the cutting force calculated by the theoretical cutting models (Miedema, Evans, Merchant or Nishimatsu) based on the volume and failure surface of the rock chip. A theoretical volume and surface is calculated based on an ideal box-shaped rock mass. A volume and surface ratio is determined.

The latest extension of the software was the dynamic model of the cutter drive train. This extension made it possible to validate the software outcome using field tests. Another important feature of this dynamic model is the potential to investigate the influence of the dynamic behavior on the excavation process. For the first time in history, the dynamics of the drive train are coupled to the cutter head and excavation process. Issues, which until now remained unanswered, can now be investigated and an explanation can be found to proof vibration phenomena. To investigate the influence of torsional vibrations, which is one of the most crucial items during rock dredging, this model can serve as a starting point.

The output of the model is a very wide range of parameters. The model calculates and stores all these parameters in a structured matrix. The most important parameters are: specific cutting energy at the cutter head, specific cutting energy at the drive, production, external torque, cutter shaft torque, drive torque, drive power, tooth forces, ladder forces, anchor forces, spud forces, RPM of the cutter head, RPM of the cutter shaft and particle size distribution. All these parameters can be plotted in time and per tooth or can be used for further calculations.

To calibrate and validate whether the interaction phenomena in the software are approximating the reality, the software was validated. This validation was performed using field tests obtained from cutter suction dredgers in practice. After validation of the model and tuning the excavation parameters in the software, more excavation cases were investigated to proof several phenomena. The field tests consisted of torque measurements performed on board two cutter suction dredgers. The first set of field tests was performed on a smaller type of cutter suction dredger. A typical 6 blades rock cutter head as well as the hard rock cutter head were tested during the excavation of hard to very hard rock types. Torque measurements were recorded on the motor end of the cutter shaft. It became clear during the tests that the hard rock cutter head was performing very well when very hard rock types were encountered. The vibration issues which were present during the excavation with a typical rock cutter head were largely disappearing during the tests with a hard rock cutter head. Using the software built, similar conditions are modeled and validated. The results were satisfying. The software was calibrated to meet the same mean torque values by varying the GSI-value of the rock mass. The torque peak to peak-value and frequency of the gradient were normative. After calibrating the model, the verification and validation of the simulation model was performed.

The field conditions encountered during the field tests were entered in the model and results were compared. Similar output values were obtained with the software for both the typical 6 blades cutter head as well as the hard rock cutter head (8 blades double action). The model proved to be stable and reliable and all variable parameters are assumed to be tuned in a realistic manner. The validation of the simulation model was continued by varying the RPM of the cutter head. A time span during the field tests was selected to validate this increase in RPM. Again, realistic results were obtained from the model. More variations in parameters are required to validate the model for other working conditions.

A final section discussed the excavation cases to measure the influence of varying input properties in the model. The influence of the different theoretical cutting models, type of cutter head, wear and shaft stiffness is investigated. The results are discussed in the next section.

5.2 Conclusions

Influence of the cutting models

The influence of the cutting models was investigated. The best results were obtained using the cutting model of Miedema. Evans, Merchant and Nishimatsu proofed to be reliable only in specific excavation cases (f.e. specific ratio rock properties UCS/BTS). The model of Miedema shows the most realistic results when considering several types of cutter head and rock parameters due to the ability of the model to switch between the tensile and shear failure state of the rock material. An intermediate state, which represents shear/tensile failure, is approximated by interpolating between both failure states for the forces as well as the breakout shapes. The ratio between average and peak cutting torque values is approximated very well during the application of the Miedema model.

Influence of the cutter heads

The influence of the cutter head type was investigated. During the modeling of the different types of cutter heads, the wear module of the software was eliminated. Different types of cutter heads were simulated in the software while excavating good quality hard rock mass. The varying parameters were the amount of blades and corresponding amount of teeth. An increasing amount of teeth and blades reduces the irregularity of the cutting process significantly. On the contrary, the average cutting torque value reached is increased due to the amount of contact points within a cutting cycle. The breakout of smaller rock parts results in an increase of tooth-rock contact. The double action cutter head seems to obtain the best performance in hard rock types. Tooth forces are within the limiting boundaries and torsional vibrations are minimized. The limited space between the blades may cause rock parts to get stuck and block the entrance of the cutter head. Although the rock parts being excavated are smaller compared to a cutter head with less blades this phenomenon may occur. A 6 blades double action cutter head or 9 blades cutter head both showed a similar performance and possess a larger space between the cutter head blades. The specific cutting energy of all cutter heads near the cutter head shows similar results.

Influence of the wear model

The wear model was implemented to incorporate the effect of the friction force on the wear surface of a cutting tooth. In the simulation model, this friction force is based on the wear area of a tooth and the UCS-value of the rock mass encountered, which is a new approach of estimating the friction force. The wear model shows increasing torque values on the cutter shaft and learns which tooth position is most susceptible to wear. The software records how many times a tooth was in contact with rock and the corresponding cutting distance traveled. A tooth is worn relative to the amount of times contact between the tooth and the rock mass, independent of the volume of rock being excavated.

Influence of the shaft stiffness

The influence of the shaft stiffness is investigated by varying the stiffness constant in the model. Two types of cutter heads were modeled while the stiffness constant was varied. More cases are required to investigate the influence in more detail, but these initial results show the impact of the shaft stiffness on the dynamic cutting process. The shaft stiffness tends to have a major impact for the 6 blades cutter head. A 6 blades cutter head, which encounters high torque fluctuations, performs better with a less stiff cutter shaft. The influence of the shaft stiffness in combination with a 9 blades cutter head is small. The peak torque values are largely diminished and the cutter shaft loading pattern is less irregular.

5.3 Recommendations

The model already shows satisfying results, although there are still several recommendations to further improve the cutter head-rock interaction. These recommendations are listed in the next paragraphs.

The heart of the cutter head-rock interaction module is the scaling of the cutting forces. These forces can now be scaled based on the volume being excavated or the surface area of the rock part. Further improvements can be made when the scaling is based on the surface cut. The difficulty lies in the determination of the exact surface cut, which is now roughly estimated by a simple algorithm. Due to the fact that a shape is constructed out of a collection of cubes, it is challenging to determine which surface area a cube, which is detected as surface cube, represents. Further development of this part of the software is required.

The interaction phenomena were only tested in the shear and shear/tensile failure zone. This due to the fact that only VOSTA cutter heads were modeled (cutting angles of 68° or higher in rock). The cutting angle has a great impact on the excavation process. It is remarkable that the Miedema cutting model states that no tensile failure can occur with a cutting angle greater than 65 degrees. Great cutting angles generate a high compressive stress near the tooth tip, making it impossible to initiate a tensile crack. For this reason, the influence of the cutting angle on the cutting process needs to be investigated. A test with a cutting angle of 45 deg (typical cutting angle during clay cutting) could be compared with the

test using a cutting angle of 68 deg (rock cutting angle). Another recommendation is to investigate the application of higher cutting angles.

The wear model was until now entered with an empirical wear rate. An optimization of the model can consist of a wear rate which is based on the fabrication steel and rock parameters. Another extension of the model can consist of defining the specific cutting energy of steel based on the empirical wear rates. The friction energy to cut a specific mass or volume of steel is already known.

The model simulates a cutter head mounted on a cutter shaft and driven by an electric drive. The dynamic behavior is modeled by a simplified mass-spring-damper system where the shaft is represented by a spring and a damper, the motor and cutter head are modeled as two end masses. Further improvements can be obtained by modeling the cutter drive train in more detail. The gearbox can be incorporated in the model and the shaft can be divided into several parts with varying stiffness. The speed control of the dynamic model is based on a typical DC-drive. A further improvement can be made by introducing the application of 3-phase AC-drive.

By further developing this model, the aim is to find upper working limits for current cutter suction dredgers excavating rock. There is a great need for a tool which allows production engineers to assess the behavior of cutter suction dredgers and cutter heads in a specific rock type. An expansion of this simulation model can consist of a sand and clay module.

Nomenclature

Acronyms

BTS	brazilian tensile strength	MPa
D-H	Denavit-Hartenberg convention	–
GSI	geological strength index	–
UCS	unconfined compressive strength	MPa

Greek Symbols

α	swing velocity corrected cutting angle of a tooth tip	rad
α_0	maximum cutting angle of a tooth tip	rad
β	shear angle of a rock failure	rad
δ	external friction angle	rad
γ	swing velocity corrected clearance angle of a tooth tip	rad
γ_0	maximum clearance angle of a tooth tip	rad
γ_0	wedge angle of a tooth tip	rad
λ	ratio between the circumferential and swing velocities	–
ϕ	internal friction angle	rad
ζ	swing velocity correction angle of a tooth tip	rad

Roman Symbols

$\vec{cd}$	cutting depth direction	–
$\vec{cv}$	cutting velocity direction	–
$\vec{le}$	leading edge direction	–
f	Miedema's interpolation coefficient between shear and tensile rock failure	–
n	Nishimatsu's stress distribution factor	–
P	pole of the orthocycloid path of a tooth tip	–
p	amount of tooth tips located at each contour line	–
R	radius of a tooth tip from the cutter head axis	m
v_{circ}	circumferential velocity of a cutter suction dredger around the working spud	rad/s
v_{cut}	cutting velocity of a tooth tip	m/s

v_{over}	cutting velocity during overcutting	m/s
v_{swing}	swing velocity of a cutter suction dredger around the working spud	m/s
v_{under}	cutting velocity during undercutting	m/s

Subscripts

acs	adapter coordinate system	–
ccs	cutter head coordinate system	–
crush	crushing	–
cut	cutting	–
ecs	earth coordinate system	–
lcs	ladder coordinate system	–
pcs	pontoon coordinate system	–
rmcs	rock matrix coordinate system	–
scs	spud coordinate system	–
tcs	tooth coordinate system	–

Bibliography

Alvarez Grima, M., Miedema, S. A., Van De Ketterij, R. G., Yenigül, N. B., and Van Rhee, C. (2015). Effect of high hyperbaric pressure on rock cutting process. *Engineering Geology*, 196:24–36.

Atilla Öztürk, C., Nasuf, E., and Bilgin, N. (2004). The assessment of rock cutability, and physical and mechanical rock properties from a texture coefficient. *The South African Institute of Mining and Metallurgy*, pages 397–402.

Cigla, M. and Ozdemir, L. (2011). Computer Modeling For Improved Production of Mechanical Excavators. Technical report, Excavation Engineering & Earth Mechanics Institute, Golden, Colorado, USA.

Claessens, S. (2008). Ontwikkeling van een freeskop voor CSD D'Artagnan (confidential). Technical report, DEME - Dredging International, Zwijndrecht, Belgium.

Claessens, S. (2009). Test campaign prototype hard rock cutter head (confidential). Technical report, DEME - Dredging International, Zwijndrecht, Belgium.

Claessens, S. and De Bosscher, L. (2016). RMPE EoW Report: 5274 - Salaya - Ambiorix - Strong rock dredging (confidential). Technical report, DEME - Dredging International, Zwijndrecht, Belgium.

de Boer, T. (1977). De Cutter. Technical report, Delft University of Technology.

Deketh, H. (1995a). The Wear Sensitive Cutting Principle of a Cutter Suction Dredge. *Terra et Aqua*, 60.

Deketh, H. (1995b). Wear of Rock Cutting Tools: Laboratory Experiments on the Abrasivity of Rock. Technical report, Delft University of Technology.

Deliac, E. (1993). Theoretical and practical rules for mechanical rock excavation. In Hudson, J., Brown, E., and Hoek, E., editors, *Comprehensive Rock Engineering*, chapter 8, pages 177–227. Pergamon Press, 4 edition.

Dredging International (2000). Dredging International Rock Cutting Formulas (confidential). Technical report, DEME - Dredging International, Zwijndrecht, Belgium.

Evans, I. (1974). Relative Efficiency of Picks and Discs for Cutting Rock. In *Proceedings 3rd Congress on Advances in Rock Mechanics*, pages 1399–1405.

Gokhan, R. and Gunes, N. (2005). A semi-empirical approach directed to cutting force prediction for point-attacker picks. *The Journal of The South African Institute of Mining and Metallurgy*, 105:257–264.

Gokhan, R. and Gunes Yilmaz, N. (2005). A new methodology for the analysis of the relationship between rock brittleness index and drag pick cutting efficiency. *The Journal of The South African Institute of Mining and Metallurgy*, 105:727–734.

Helmons, R. and Miedema, S. (2013). Cutting through hard rock-like materials-a review of the process. In *WODCON XX: The Art of Dredging*, Brussels, Belgium. WODA, World Organization of Dredging Associations.

Hignett, H. and Banks, D. (1985). Current Issues in Rock Dredging. pages 321–333.

Hoek, E. (2006). *Practical Rock Engineering*. North Vancouver, British Columbia, Canada, first edition.

Hood, M. and Roxborough, F. (1992). Rock Breakage: Mechanical. In Society for Mining, M. and Exploration, editors, *SME Mining Engineering Handbook*, pages 680–721. Littleton, Colorado, USA.

http://mathworld.wolfram.com (2016). Wolfram Mathworld.

http://www.deme-group.com (2016). DEME.

Hughes, H. (1969). Mechanized stone work. *The Mining Engineer*, pages 689–692.

Jakobsen, P. and Mao, D. (2013). Rock-Bit Interaction: review of models (confidential). Technical report, SINTEF Building and Infrastructure, Trondheim, Norway.

Kuidong, G., Changlong, D., Hongxiang, J., and Songyong, L. (2014). A theoretical model for predicting the Peak Cutting Force of conical picks. *Frattura ed Integrita Strutturale*.

Lagace, P. (2008). Unified handout materials and structures.

Lindqvist, P. and Hai-Hui, L. (1984). Behavior of the Crushed Rock Zone. Technical Note. In *Rock Mechanics and Rock Engineering*, chapter 16, pages 199–207.

MarCom Working Group 144 (2014). *Classification of soils and Rocks for the Maritime Dredging Process*. PIANC secrétariat général, Brussels, 1st edition.

Marin (2003). Soil Reaction Forces DREDSIM 2000.

Marinos, V., Marinos, P., and Hoek, E. (2005). The geological strength index: Applications and limitations. *Bulletin of Engineering Geology and the Environment*.

Menezes, P. L., Lovell, M. R., Avdeev, I. V., and Higgs, C. F. (2014). Studies on the formation of discontinuous rock fragments during cutting operation. *International Journal of Rock Mechanics and Mining Sciences*.

Miedema, S. (2003). Modeling of the Swing Winches of a Cutter Dredge in Relation to Simulators. Technical report, Delft University of Technology, Delft, The Netherlands.

Miedema, S. (2009). New Developments Of Cutting Theories With Respect To Dredging The Cutting Of Clay. In *WEDA XXIX & Texas A&M 40*, Phoenix Arizona, USA.

Miedema, S. (2014). *The Delft Sand, Clay and Rock Cutting Model*. Delft University Press, Delft, first edition.

Miedema, S. (2015). *The Delft Sand, Clay and Rock Cutting Model*. Delft University Press, Delft, third edition.

Mishnaevsky, L. and Mpa, J. (1998). Rock fragmentation and optimization of drilling tools. *Computational Mechanics Publications*, pages 167–203.

Nishimatsu, Y. (1972). The Mechanics of Rock Cutting. *International Journal of Rock Mechanics and Mining Science*, 9:261–270.

Pickering, R. and Ebner, B. (2002). Hard rock cutting and the development of a continuous mining machine for narrow platinum reefs. *The South African Institute of Mining and Metallurgy*.

Prieto, L. and Verna, T. (2013). Cuttability and Abrasivity of Rocks in Capital Dredging. In *WODCON XX: The Art of Dredging*, Brussels, Belgium. WODA, World Organization of Dredging Associations.

Ramezanzadeh, A. and Hood, M. (2010). A state-of-the-art review of mechanical rock excavation technologies. *International Journal of Mining and Environmental Issues*, 1(1):29–39.

Rise, T., Bergh, I. S. B., Dahl, F., and Jakobsen, P. (2013). (R)Evolution from soft to hard rock cutter dredging (confidential). Technical report, SINTEF Building and Infrastructure, Trondheim, Norway.

Rojek, J. (2010). Simulation of rock cutting with the Discrete Element Method (DEM) Outline of the presentation. pages 9–10.

Sewlal, B. (2012). Construction Report: Cutter Drive D'Artagnan (confidential). Technical report, IHC, Kinderdijk.

Siva Sanker, U. (2015). Rock Excavation Systems Mechanical Excavation: Theories of Interaction of Rock Cutting tools Rock Breaking Processes. Technical report, Singareni Collieries Company Ltd.

Thuro, K. and Plinninger, R. J. (2003). Hard rock tunnel boring, cutting, drilling and blasting: rock parameters for excavatability. *South African Institute of Mining and Metallurgy*.

Tiryaki, B., Ayhan, M., and Hekimoğlu, O. Z. (2001). A New Computer Program for Cutting Head Design of Roadheaders and Drum Shearers. pages 975–395.

USDAT, D. o. D. (2009). DoD Modeling and Simulation (M&S) Verification, Validation, and Accreditation. *DoD Instruction 5000.61*, pages 1–10.

van der Krogt, J. (2004). Torsional vibration analysis cutter drive (confidential). Technical report, IHC, Kinderdijk.

van Es, A. (2000a). Gedrag van een cutterzuiger tijdens het snijden van gesteenten: modellering. Technical report, Delft University of Technology.

van Es, A. (2000b). Onderzoek en modellering van het dynamisch gedrag van een cutterzuiger tijdens het snijden van gesteenten: literatuuronderzoek. Technical report, Delft University of Technology.

Vereniging van Waterbouwers (2010). 5a: Cutter Suction Dredger. In van't Hoff, J., editor, *Advanced Training Hydraulic Engineering Works*. Association of Dredging Contractors, Gouda.

Verhoef, P. (1997). *Wear of Rock Cutting Tools: Implications for the site investigation of rock dredging projects*. PhD thesis, Delft University of Technology.

Vlasblom, W. J. (2003). Lecture WB3413 Dredging Processes Cutting of Rock. Technical report, Delft University of Technology, Delft, The Netherlands.

Weller, A. (1966). Het graafproces van een cutterzuiger. Technical report, Delft University of Technology.

Whittaker, B., Singh, R., and Sun, G. (1992). *Rock Fracture Mechanics*. Elsevier, Nottingham, U.K.

Wijma, K. (2008). Dredge cutterheads for 100-150 Mpa. Technical report, VOSTA LMG, Haarlem, The Netherlands.

www.electrical4u.com (2016). electrical4u.

www.openelectrical.org (2015). OpenElectrical.

Yasheng, M. and Fusheng, N. (2006). Calculation of the Blade Cutting Force for small Cutting Angles based on MATLAB. *Water*.

List of Figures

List of Tables